5-2017

Vehicle Parameters Estimation and Driver Behavior Classification for Adaptive Shift Strategy of Heavy Duty Vehicles

Darui Zhang
Clemson University, daruiz@g.clemson.edu

VEHICLE PARAMETERS ESTIMATION AND DRIVER BEHAVIOR CLASSIFICATION FOR ADAPTIVE SHIFT STRATEGY OF HEAVY DUTY VEHICLES

A Dissertation
Presented to
the Graduate School of
Clemson University

In Partial Fulfillment
of the Requirements for the Degree
Doctor of Philosophy
Automotive Engineering

---

by
Darui Zhang
May 2017

Accepted by:
Zoran Filipi, Committee Chair
Andrej Ivanco, Co-chair, Research Advisor
Beshah Ayalew
Robert Schalkoff

ABSTRACT

Commercial vehicles fulfill the majority of inland freight transportation in the United States, and they are very large consumers of fuels. The increasingly stringent regulation on greenhouse-gas emission has driven manufacturers to adopt new fuel efficient technologies. Among others, advanced transmission control strategy can provide tangible improvement with low incremental cost. An adaptive shift strategy is proposed in this work to optimize the shift maps on-the-fly based on the road load and driver behavior while reducing the initial calibration efforts. In addition, the adaptive shift strategy provides the fleet owner a mean to select a tradeoff between fuel economy and drivability, since the drivers are often not the owner of the vehicle.

In an attempt to develop the adaptive shift strategy, the vehicle parameters and driver behavior need to be evaluated first. Therefore, three research questions are addressed in this dissertation: (i) vehicle parameters estimation; (ii) driver behavior classification; (iii) online shift strategy adaption.

In vehicle parameters estimation, a model-based vehicle rolling resistance and aerodynamic drag coefficient online estimator is proposed. A new Weighted Recursive Least Square algorithm was developed. It uses a supervisor to extracts data during the constant-speed event and saves the average road load at each speed segment. The algorithm was tested in the simulation with real-world driving data. The results have shown a more robust performance compared with the original Recursive Least Square algorithm, and high accuracy of aerodynamic drag estimation.

To classify the driver behavior, a driver score algorithm was proposed. A new method is developed to represent the time-series driving data into events represented by symbolic data. The algorithm is tested with real-world driving data and shows a high classification accuracy across different vehicles and driving cycles.

Finally, a new adaptive shift scheme was developed, which synthesizes the information about vehicle parameters and driver score developed in the previous steps. The driver score is used as a proxy to match the driving characteristics in real time. Drivability objective is included in the optimization through a torque reserve and it is subsequently evaluated via a newly developed metric. The impact of the shift maps on the objective drivability and fuel economy metrics is evaluated quantitatively in the vehicle simulation.

The algorithms proposed in this dissertation are developed with practical implementation in mind. The methods can reduce the initial calibration effort and provide the fleet owner a mean to select an appropriate tradeoff between fuel economy and drivability depending on the vocation.

ACKNOWLEDGMENTS

I would like to thank many people I have worked with during my Ph.D. program.

First and foremost, I would thank my research advisor and friend Dr. Andrej Ivanco, without who my progress would not be possible. Next, I would thank for my committee Chair Dr. Zoran Filipi, for giving me precious guidance and support. Thanks to my committee members Dr. Beshah Ayalew, and Dr. Robert Schalkoff, whose insightful comments made finishing the dissertation an enriching experience.

I would thank Andy Byerly and Nicholas McDonough from Allison Transmission for providing valuable feedback and collecting the data in this research while supporting my work through a sponsored research agreement. Also, I would also like to thank other faculties I had the privilege to know and work with at Clemson, foremost Dr. Robert Prucka, Dr. Ardalan Vahidi, and James Potter.

Also thanks to the many friends that I have met over these years: Qian Wang, Bin Xu, Zhe Wang, Ting Zheng, Zhiyuan Du, Zeren Xu, Xiaoyan Yu, Zifan Liu, Jasmine Wood, Adamu Yebi, and Bashar Alzuwayer.

Finally, thanks to my parents Guogang Zhang and Yuqin Li who have raised me to have a curious mind and supported me over the years.

TABLE OF CONTENTS

Page

Table of Contents (Continued)

Page

LIST OF TABLES

LIST OF FIGURES

List of Figures (Continued)

Figure Page

List of Figures (Continued)

Figure Page

CHAPTER ONE

INTRODUCTION

Commercial vehicles contribute to the 74 percent of the freight transportation in the United States [1]. They are also large fuel consumer. An average medium and heavy duty truck drives 13,100 miles per year and uses 1,800 gallons of fuel [2]. The increasingly stringent greenhouse gas emission regulations [3] stimulate the adoption of new fuel-saving technologies [4]. Among them, the advanced transmission shift strategy plays an important role in the powertrain system [5].

1.1 The Role of Transmission Shift Strategy in the Powertrain

The transmission plays a major role in the vehicle powertrain system. Due to the limited range of speed and torque of the internal combustion engine, the transmission is needed to mediate the engine power and the road load [6].

The transmission shift strategy determines the gear ratio between the engine the output shaft [7]. The gear ratio can be discrete or continuous (known as the Continuously Variable Transmission). For the same output power, different gear ratio will result in engine operation at different speed/torque points. The engine's fuel efficiency can vary largely depending on the operational region [8]. Therefore, the transmission shift scheduling is crucial to the engine's fuel efficiency.

The responsiveness of the driver feeling is referred as the drivability [9][10]. The drivability is closely related to the torque reserve, which is defined as the capability of the additional torque the engine can provide without downshifting, as described in the study

by Viet [11]. The trade-off between the driveability and fuel economy often presents a challenge in calibrating the shift strategy, because the most fuel-efficient engine operating region is usually near the maximum torque line, where the torque reserve is low. As a result, allocating too much torque reserve will lead to low fuel economy, because the engine will operate in its less fuel-efficient region. On the other hand, too little torque reserve will cause the vehicle to feel less responsive. A good shift strategy needs to balance the two contradictory attributes and often requires extensive calibration.

1.2 Motivation for Adaptive Shift Strategy

The conventional shift strategy is realized by a shift map based on vehicle speed and throttle position. The map often requires extensive calibration to different vehicle types and applications, as described in the study by Newman et al.[12]. Unlike passenger cars, in which the vehicle parameters have more certainty, commercial vehicles can have multiple vehicle configurations. For example, a fleet of commercial vehicles can have various engine-transmission-body combinations; each vehicle can also be equipped with different components (e.g. aerodynamically enhanced trailers and low rolling resistance tires). Further, the vehicle parameters are often subjected to change in situations such as loading on/off a trailer. The wide variety of vehicle parameters creates the needs for online vehicle parameters estimation. This in turn will enable development of the methodology for adapting the shift strategy to current vehicle configuration and driving conditions, allows the shift strategy to automatically adjust to the different vehicle parameters.

Another challenge of the conventional shift strategy is that the commercial vehicles operate for a variety of vocations, which have different requirement for fuel economy and drivability. For example, delivery trucks might place more emphasis on drivability to improve productivity; on the contrary, owner of the semi-trailer trucks might be more interested in reducing fuel cost. Therefore, the shift map often requires extensive calibration to different applications.

In addition, the drivers are often not the owners of the vehicles. Unnecessary aggressive driving behavior can result in a large increase in fuel consumption and greater cost to fleet owner. The study by Sivak and Schoettle has shown driver aggressiveness can contribute the 20 percent difference in fuel economy in real-world driving [13]. One way to reduce the initial transmission calibration effort and increase fuel economy is to adapt the shift strategy based on the drivability target and the actual driver behavior.

With respect to challenges posed by the wide variety of vehicle configurations and the different driver behavior, the adaptive shift strategy has been introduced. It utilizes multiple shift maps, which are optimized for various vehicle road load and fuel economy target and can adjust the shift map to the different vehicle parameters and driver behavior on the fly, which can potentially reduce the initial calibration efforts and improve fuel economy. On the other hand, the scheme requires the online estimation of road load and driver behavior as an adaptation prerequisite.

1.3 Goals of this Work

In order to improve vehicle fuel economy and reduce the initial calibration effort, it is important for the transmission controller to evaluate the road load and driver behavior and adjust the shift strategy on the fly. The road load estimation and driver behavior classification are treated as two tasks to be solved separately. Lastly, an adaptive shift strategy will be proposed which optimized the shift map based on the information of vehicle parameters and driver behavior on-the-fly to achieve the desired fuel economy and drivability.

To summarize the above discussion, the goal of this dissertation is to develop algorithms that:

1) Estimate vehicle parameters online to calculate vehicle road load.
2) Classify driver behavior to adjust the torque reserve to the driver expectations.
3) Synthesis vehicle parameters and driver behavior in the adaptive shift strategy and evaluate the benefit through objective metrics of drivability and fuel economy.

1.4 Thesis Organization

The remainder of this dissertation is organized as follows:

1) Chapter Two reviews the related work conducted in previous studies.
2) Chapter Three summarizes the contributions of this dissertation.
3) Chapter Four extends the prior work on vehicle parameters estimation and proposes a new algorithm to estimate vehicle rolling resistance and aerodynamic drag coefficient

online based on the vehicle longitudinal dynamic model during the constant-speed event.

4) Chapter Five covers driver behavior evaluation, and development of the driver scoring algorithm based on supervised learning.
5) Chapter Six proposes an adaptive shift strategy, which utilizes the vehicle parameters and driver score to estimate the driver demand.
6) Chapter Seven concludes the study and discusses the direction for the future work.

CHAPTER TWO

RELATED WORK OF OTHERS

2.1 Vehicle Road Load Estimation

The transmission shift strategy can be optimized when the information of vehicle road load is known. The vehicle road load estimation requires information about several vehicle parameters, including vehicle mass, road grade, rolling resistance and aerodynamic drag coefficient. Over the past decades, there has been a profusion of research on model-based methods for vehicle parameters estimation, due to its broad application in powertrain controls, e.g. transmission shift strategy [14], adaptive cruise-control [15] and look-ahead controls [16].

Numerous studies have been devoted to vehicle mass estimation, because of its preeminent influence on the road load of heavy vehicles, especially during accelerating and hill climbing. Among many approaches to estimate vehicle mass [17], the model-based approach through the longitudinal dynamic is most commonly used. The advantage is that it requires minimal additional sensors [18] and most of the signals needed for estimation can be obtained from the Control Area Network (CAN) bus on the vehicle [19].

Road grade estimation has also been investigated. The previous approaches can be categorized into sensor-based and model-based. The sensor-based approach uses various sensors to measure the road grade, such as GPS [20], barometer [21] and inclinometer

[22]. The measurements from the sensors are usually noisy: GPS and barometer have a coarse resolution; inclinometer is very susceptible to motion. Therefore, the measurements from one or more sensors are often combined with a model-based filter to improve the accuracy. The simultaneous estimation of mass and road grade using the model-based approach is a more difficult task due to the time-varying nature of the road grade [23]. To address the problem, adaptive observers have been proposed in [24][25].

A frequently used algorithm in the literature includes Recursive Least Squares (RLS), RLS with forgetting factor and Kalman filter. RLS is suited for estimating constants, such as vehicle mass[18]. A variation of the RLS method is the RLS with forgetting factor, which is suited for estimating parameters that change slowly, such as the road grade[26]. Kalman filter is suitable for problems in which the dynamics of the parameters are known [27][28][29].

Several studies use the event-seeking approach, which monitoring vehicle motion and extract data only during certain events [17][30][31]. The events include sharp accelerating, decelerating and gear shifting. The advantage of the event-seeking approach is that the signal acquired during the selected events usually have higher signal-to-noise ratio.

Rolling resistance and aerodynamic drag coefficient is commonly estimated offline using the coast-down test [32][33]. In the study by Mayer and Wiedemann [34], a measuring trailer was used to measure the rolling resistance. An online model-based estimation approach has been proposed in [18] using signals from the CAN bus. The method shows high accuracy of mass estimation, however, the accuracy of rolling

resistance and still need to be improved. This is because rolling resistance and aerodynamic drag are relatively lower than mass related inertia force and therefore more sensitive to noise in the input signals. Simultaneous estimation of rolling resistance and aerodynamic drag coefficient parameters requires a large variation of vehicle speed to achieve a high accuracy. The study by Andersson used an Extended Kalman filter to estimate rolling resistance or aerodynamic drag coefficient one parameter at a time [35].

The rolling resistance and aerodynamic drag coefficient are key parameters to predict the vehicle road load. The supervisory data extraction scheme is a promising approach to further improve the accuracy of the simultaneous estimation of the parameters.

2.2 Eco-driving and Driver Behavior Classification

Real-world fuel economy largely depends on driver behavior. Aggressive driving behaviors (e.g. abrupt acceleration and braking) have little effect on reducing trip duration. However, it will considerably increase fuel consumption. On the other hand, studies have shown fuel economy can be improved up to 20-30 percent by using eco-driving techniques [13].

Ecological driving, or eco-driving, behavior has been investigated in the recent decades, due to the rising concern of the fuel economy [36]. The information about driver behavior has an extensive application in driver assistance systems, as reviewed in the study by Wada et al.[37] and Vagg et al.[38]. It can also improve the powertrain controls, such as the throttle control and shift strategy in the conventional vehicle [39], the energy

management system in hybrid vehicles [40][41] and range estimation for electric vehicle [42]. Several approaches focus on the use of optimal control to minimize the fuel consumption [43][44]. The optimized powertrain control policy takes account the traffic flow, road grade and the historical driving data to reduce the fuel consumption [45][46][47][48].

The methods of classifying driver behavior can be grouped into three categories: rule-based methods, supervised learning, and unsupervised learning. Rule-based methods classify the driver behavior based on criteria such as accelerating and pedal position. Previous studies have used the fuzzy logics method, based on the patterns from the vehicle load [49], and the acceleration-speed diagram [50]. The study by Manzoni et al.[51] uses an index defined based on the real and ideal fuel consumption. The major disadvantage of the rule-based method is that parameters in the classification rules need to be manually validated, which can be increasingly difficult as the complexity of the problems increases.

Supervised learning can automatically determine the parameters from the data. The category of supervised-learning method includes many algorithms. For example, decision trees and logistic regression have been used in [52] to classify driving events; artificial neural network and Support Vector Machine (SVM) have been used in [53], to determine drivers' handling skills. SVM have been used to investigate driver behavior at the intersection in the study by Aoude et al.[54]. Further, graphical models (e.g. the Hidden Markov Model) have also been demonstrated in the previous research to predict

driving behaviors [55][56][57]. However, the limitation of supervised-learning methods is that they require labeled data, which may be scarce and expensive to collect.

Unsupervised learning is preferred where the unlabeled data is abundant. The most common application of unsupervised learning methods is clustering. In that case, unlabeled driving data is grouped into classes of different driving behavior base on their similarity in certain features. C-means and PCA (Principal Component Analysis) have been used in the study by Constantinescu et al.[54] and Kedar-Dongarkar and Das [55]. The drawback of unsupervised learning method is that the ground truth is not available. Therefore, it is better suited for data exploration.

The driver behavior classification typically proceeds in two stages: feature extraction and classification. The feature extraction stage comprises determining the duration of a classification event and extracting features from the time-series driving data. The classification stage usually involves applying the standard classification algorithms to the dataset. The feature extraction stage is considered more challenging.

The driving data is typically in the form of time-series [60]. Vehicle longitudinal motion can be obtained from the Controller Area Network (CAN) bus; lateral motion can be acquired from steering angle and yaw sensor; the vehicle following distance can be measured by the radar sensor [61]. Regarding the eco-driving behavior, the signals related to vehicle longitudinal motion is the most relevant [51][62][63] (e.g. vehicle speed, acceleration, throttle, and pedal position). In this section, we use only the signals from the CAN bus without any additional sensors.

The most commonly used features in the literature are extracted from the statistical

analysis and frequency content of the driving data. Features from the statically analysis include the average, percentile and standard deviation, etc.[62][64][65]. The study by Ericsson [66] has summarized various factors that can affect the driving patterns using statistical inference analysis. One of the disadvantages of using the statistical features is that the features are usually route-dependent. The statistical values of the driving data are only comparable with the similar routes. Features from the frequency content are another type of commonly used features, which seek patterns in the signals' spectral density obtained by the Fast Fourier Transformation (FFT) [67][68]. The method is usually more computationally demanding, and therefore, better suited for off-line analysis. In contrast to the prior art, we propose an algorithm which converts the time-series driving data into events represented by symbolic data to improve the computational and memory efficiency. Determining the duration of classification is another challenge. The literature primarily relies the analysis on an entire driving cycle [69][58].

To summarize, supervised learning is a promising approach for driver behavior classification, because driving behaviors are implicit and ambiguous. Previous studies have used features based on the statistical and frequency analysis of the driving data. However, the robustness of the schemes across different vehicles and driving cycles still leaves room for improvement.

2.3 Transmission Shift Strategy

The shift strategy controls the gear ratio between the engine the output shaft and determines the engine operating points. Therefore, it is crucial to the vehicle fuel consumption and drivability.

In addition to the conventional shift map based on vehicle speed and throttle position [6], several alternative methods for developing shift strategy have been proposed to allow the flexibility under different situations including Fuzzy Logic, Neural Network, and Dynamic Programming. The Fuzzy Logic based shift strategy allows some flexibility for factors such as the vehicle load, hill climbing and driving behavior [70][71][72]. However, the drawbacks of the method are the difficulty in achieving high accuracy calibration. The Neural Network approach allows the shift strategy to adjust to several parameters as well [39]. For example, the steering angle, braking force, vehicle speed, road grade, and the dynamics of the engine operation [73][74]. However, the disadvantage is that the decisions about weights and biases determined during training lack system transparency.

The Dynamic Programming based approach has been demonstrated by several recent studies[11][75]. The optimal shift strategy can be found based on the knowledge of the upcoming driving demand. Look ahead control has been studied by Hellström et al. [76], using the preview of the road load information such as the road grade. The model predictive control approach has been proposed by Ngo et al. [77], based on the prediction of future driving demand of a driving cycle. The method requires the information of the future road demand which is often unknown. As a result, it is often used as the

benchmark [11]. Though the stochastic dynamic programming, which based on the probabilistic prediction of the further driving demand, is real-time implementable, the prediction of the future load demand requires further investigation. The study by Ngo et al. [78] compared the optimal gearshift strategies generated by dynamic programming using three methods (weighted inverse of power reserve, constant power reserve, and variable power reserve) and stochastic dynamic programming. The Stochastic Dynamic Programming is real-time implementable, and the simulation results show on average it has nearly equal performance on the fuel consumption.

The map-based shift strategy is still the preeminent method used in vehicles today, owing to its simplicity in implementation and calibration. Improvements have been made to the conventional shifting map. The shift map considering vehicle mass has been proposed in the study by Yong and Jian [79] and the power-based shift map has been demonstrated in the study by Bai et al. [6]. A neural network based adaptive shifting strategy has been proposed by Kondo and Goka [39], which uses various maps adjusted by factors regarding vehicle load and driver behavior. The optimization of the shift map is a complex process, in which several factors need to be considered including the fuel consumption, drivability, and emission [80]. The drivability is associated with the driver's experience and the brand essence. Therefore it is in part subjective and hard to quantify. Several studies have attempted to use objective metrics to quantify drivability [81][82][83][84]. The most common metrics is related to the driving comfort and the operating smoothness and responsiveness [85].

To summarize, the adaptive shift strategies, which can automatically adjust the shift points to the vehicle parameters and driver behavior, have not been sufficiently addressed in published literature and requires further study.

CHAPTER THREE

CONTRIBUTIONS

3.1 Contributions

The adaptive shift strategy is a cost-effective method for potentially reduction of initial calibration effort and the real-world fuel consumption. However, it requires the information about vehicle parameters and driver behavior. In this dissertation, we develop new algorithms for estimating the vehicle parameters and evaluating the driver behavior in real-time. Subsequently, adaptive shift strategy is proposed to adjust the shift map on the fly and provide a way for the fleet owner to choose between fuel consumption and drivability.

A model-based estimation algorithm is proposed to estimate vehicle rolling resistance and aerodynamic drag coefficient, which have not been much studied in the literature. The scheme estimates rolling resistance and aerodynamic drag during the constant-speed events. To address the issue of lack of persistence of excitation during constant-speed, the Weighted Recursive Least Square algorithm is developed. The algorithm is tested with real-world driving data. Results show more robust performance than the original Recursive Least Square Algorithm.

A driver score algorithm was proposed to evaluate the driver behavior. A new method is developed to represent the time-series driving data into events by represented symbolic data. The classification is conducted based on microtrips, which to the best of

our knowledge have not be studied before. The algorithm is tested with real-world driving data from different vehicle configurations and shows a high classification accuracy.

Lastly, the new adaptive shift scheme was proposed, which synthesizes the information about vehicle parameters and driver score. The shift map is optimized based on the characteristics of the driving cycle, which is approximated from the driver score. The effect of the shift maps on the objective drivability and fuel consumption metrics is evaluated using the vehicle simulation. The adaptive shift strategy provides the fleet owner a way to choose between the fuel consumption and drivability.

The algorithms have low computational overhead, which increases linearly with the number of samples, and constant memory requirement. Thus, it is applicable to Transmission Control Unit (TCU).

3.2 Publications

The research involving this dissertation has been presented at a number of international conferences and published in refereed journals. The publications are listed below:

1) D. Zhang, and A. Ivanco, "Adaptive Transmission Shift Strategy based on Online Characterization of Driver Aggressiveness," *SAE International Journal of Commercial Vehicles (Work in Progress)*
2) D. Zhang, and A. Ivanco, "Real-time Eco-driving Behavior Classification based on Microtrips," *IEEE Transactions on Intelligent Vehicles (Under Review)*

3) D. Zhang, A. Ivanco, Z. Filipi, and A. Vahidi, “Event-based Aerodynamic Drag and Rolling Resistance Estimation Using Weighted Recursive Least Squares Algorithm,” *Vehicle System Dynamics Taylor & Francis (Under Review)*

4) D. Zhang, B. Xu, and J. Wood, “Predict failures in production lines: A two-stage approach with clustering and supervised learning,” *2016 IEEE International Conference on Big Data*, pp. 2070-2074, 2016.

5) D. Zhang, A. Ivanco, and Z. Filipi, “Model-Based Estimation of Vehicle Aerodynamic Drag and Rolling Resistance,” *SAE International Journal of Commercial Vehicles*, *8*(2), 433-439, 2015. (*Student Paper Award*)

6) D. Zhang, A. Ivanco, and Z. Filipi, “An Averaging Approach to Estimate Urban Traffic Speed Using Large-scale Origin-destination Data,” *International Journal of Powertrains*, *4*(2), 126-140, 2015.

CHAPTER FOUR

VEHICLE PARAMETERS ESTIMATION

4.1 Introduction

Vehicle road load estimation requires knowledge about key vehicle parameters, including vehicle mass, road grade, rolling resistance and aerodynamic drag coefficient. Unlike passenger cars, the parameters of a commercial vehicle are more uncertain. Commercial vehicles can have many engine-transmission-body combinations and use various components such as aerodynamically-enhanced trailers and low rolling resistance tires. To reduce the initial calibration effort, the vehicle parameters can be estimated online to allow the powertrain controllers to adapt to the different vehicle configurations.

The online estimation of vehicle mass and road grade has been successfully demonstrated in the past, but the estimation of the vehicle rolling resistance and aerodynamic drag coefficient requires further attention. Simultaneously estimating the rolling resistance and aerodynamic drag coefficient requires large variation of vehicle speed, which is difficult to obtain in the real-world driving situation. In this section, a Weighted Recursive Least Square algorithm is proposed to overcome the limitation by storing and updating the road load in different speed segments. The algorithm had shown a more robust performance compared with the original Recursive Least Square algorithm.

4.2 Estimation Scheme

The estimation scheme consists of three major steps as shown in Fig.4.1, i.e. identifying driving events, updating measurements in speed segments, and estimating the vehicle parameters. A supervisor continuously monitors the driving situations and extracts data only in the events with high signal to noise ratio. When the data extraction criteria are satisfied, the algorithm updates the average road load at the current speed interval. Finally, the algorithm obtains the estimation of rolling resistance and aerodynamic drag coefficient using the average road load at different speed segments. The details of the steps are explained in this section.

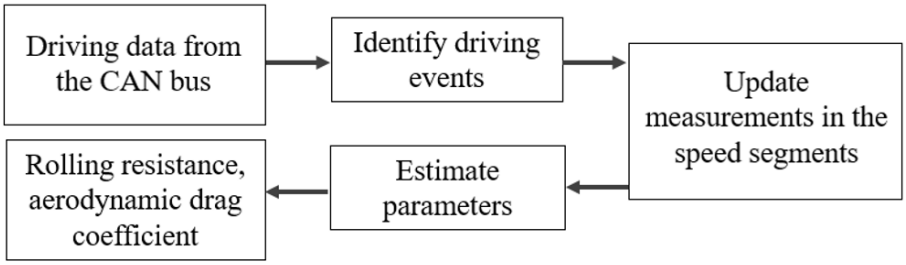

Fig. 4.1 Schematic flow chart of the vehicle parameters estimation process

4.2.1 Longitudinal Vehicle Dynamic

The vehicle model is based on the longitudinal quasi-static vehicle dynamic model. The following assumptions have been made: i) the vehicle motion is predominantly longitudinal and therefore the lateral forces are neglected; ii) wheel slip is not present between the tire and the road surface; iii) the braking force is not applied; iv) the effects of wind gusts are neglected. The vehicle longitudinal forces [86] are shown in Fig.4.2.

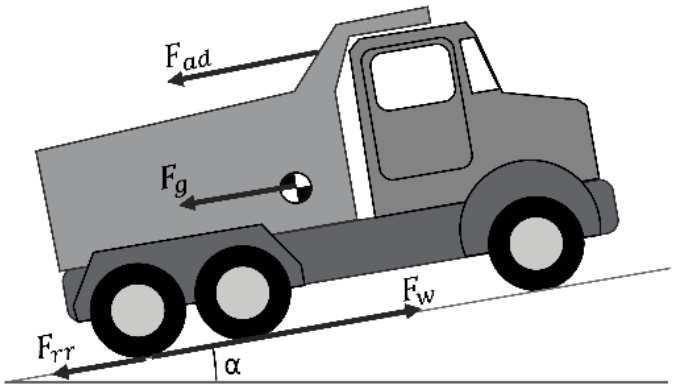

Fig.4.2 Vehicle longitudinal forces

The vehicle longitudinal dynamics during the quasi-static state is described in equation (4.1).

$$ma = F_w - F_r - F_{ad} - F_g \qquad (4.1)$$

where the wheel traction force F_w consists of four components: aerodynamic drag F_{ad}, rolling resistance F_r, grade force F_g, and acceleration resistance ma. Each force can be calculated as follows:

$$F_w = \frac{T_e \omega_e \eta}{v} \qquad (4.2)$$

$$F_{ad} = \frac{1}{2} A \rho C_d v^2 \triangleq C_{dL} v^2 \qquad (4.3)$$

$$F_g = mg \sin(\alpha) \approx mg\alpha \qquad (4.4)$$

$$F_r = mgC_r \cos(\alpha) \approx mgC_r \qquad (4.5)$$

where the wheel traction force F_w can be calculated from the engine torque T_e, engine speed ω_e, overall powertrain η efficiency, and vehicle speed v. The relationship is based on the assumption that the vehicle is in the quasi-static state, and the wheel slip does not occur. In (4.3), the vehicle frontal area A, air density ρ and aerodynamic drag coefficient C_d can be lumped together in a single term C_{dL}, which determines the aerodynamic drag. The grade force F_g and rolling resistance F_r can be written as in (4.4) and (4.5) respectively, when the road grade α is small. The rolling resistance coefficient C_r is modeled as a constant in (4.5). Although rolling resistance coefficient increases nonlinearly with vehicle speed, the value remains mostly constant below 100 km/h [87].

Equation (4.6) can be obtained by combining equation (4.1) to (4.5).

$$\frac{T_e \omega_e \eta}{v} - ma - mg\alpha = \hat{C}_{dL} v^2 + \hat{F}_{rr} \qquad (4.6)$$

The right-hand side of the equation consists of rolling resistance and aerodynamic drag. It can be seen as the basic road load, which indicates the force needed for the vehicle to maintain its current speed without accelerating and overcoming road grade. The equation (4.6) can be written in the linear form based on the definition of parameters in equation (4.7).

$$y = \phi \hat{\theta} \qquad (4.7)$$

$$y = \frac{T_e \omega_e \eta}{v} - ma - mg\alpha \qquad (4.8)$$

$$\phi = [v^2 \quad 1] \qquad (4.9)$$

$$\hat{\theta} = [\hat{C}_{dL} \quad \hat{F}_r]^T \in \mathbb{R}^2 \qquad (4.10)$$

Where $\hat{\theta}$ is the parameters to be estimated including aerodynamic drag coefficient $\hat{C}_{dL}$and rolling resistance $\hat{F}_r$. The input signals include engine speed ω_e, engine torque T_e, vehicle speed v, longitudinal acceleration a, vehicle mass m and road grade α.

4.2.2 Identification of Driving Events

A supervisor is needed to continuously monitor the vehicle driving situation and extract data only during events which have high signal-to-noise ratio, as shown in Fig.4.3. The data extraction criteria include the following aspects:

1) The vehicle is driving at a relatively constant speed, which is determined by a threshold in the longitudinal acceleration.
2) The vehicle motion is predominantly longitudinal, which is defined by a threshold in the lateral acceleration.
3) The vehicle is not braking, which is indicated by the brake on/off signal. iv) The vehicle speed needs to be higher than a lower limit.

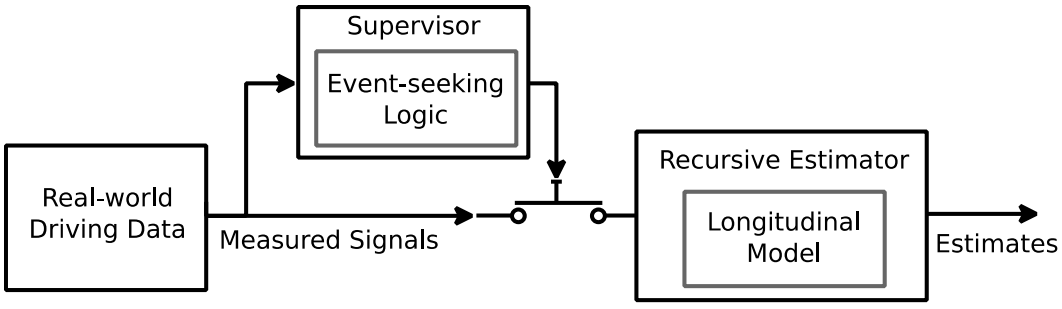

Fig. 4.3. Illustrating the supervisory data extraction scheme

Firstly, during constant-speed driving, the rolling resistance and aerodynamic drag accounts for the majority of the road load and the error brought by the acceleration is minimal. In contrast, during sharp acceleration, the majority of the road load consists of the acceleration resistance. Obviously, only the constant-speed driving is suitable for estimating the rolling resistance and aerodynamic drag coefficient. Secondly, the supervisor extracts data only when the vehicle motion is predominantly longitudinal because the model-based estimator only considers the longitudinal motion. Thirdly, while the brake force would ideally be estimated from the clamping force of the brake pads, only the brake on/off signal was available in experiments. Therefore, the algorithm only considers the data when the brake is not activated. Finally, the algorithm exclude the data obtained at low speed, because it can have more uncertainty due to the torque converter.

4.2.3 Measurement Update

The vehicle speed trace is discretized into segments. The road load measurement in each segment is represented as a 2-tuple $(\bar{y}_i, n_i)$, where $\bar{y}_i$ is the average road load, and n_i is the number of measurements in the segment i. The collection $\bar{y}_i$ and n_i of all the segments are represented as $Y$and N. The steps of the algorithm is shown in the Appendix, Alg.4.1.

In step 1, the algorithm checks if the current driving event satisfies the data extraction criteria which is described in section 4.3.2. In step 2, the algorithm computes the road load y from the input signals using equation (4.8). In step 3, the algorithm determines the speed segment i for this measurement, based on which speed interval the current speed falls into. In step 4, the algorithm adjusts the road load based on the

difference between the vehicle speed and the segment speed as shown in equation (4.11) and (4.12).

$$\Delta y = \tilde{C}_{dL}(v_i^2 - v^2) \approx 2\tilde{C}_{dL} v_i \Delta v \qquad (4.11)$$

$$y_i = y + \Delta y \qquad (4.12)$$

Where $\tilde{C}_{dL}$ is the approximated aerodynamic coefficient, v_i is the middle speed of the segment i, v is the vehicle speed, and Δv the difference of between the vehicle speed and segment speed. The adjustment reduces the approximation error introduced by discretizing the speed intervals. A similar amount of data will normally fall above and below a segment speed, which will even out the error when averaging them together. The process is illustrated as shown in Fig.4.4.

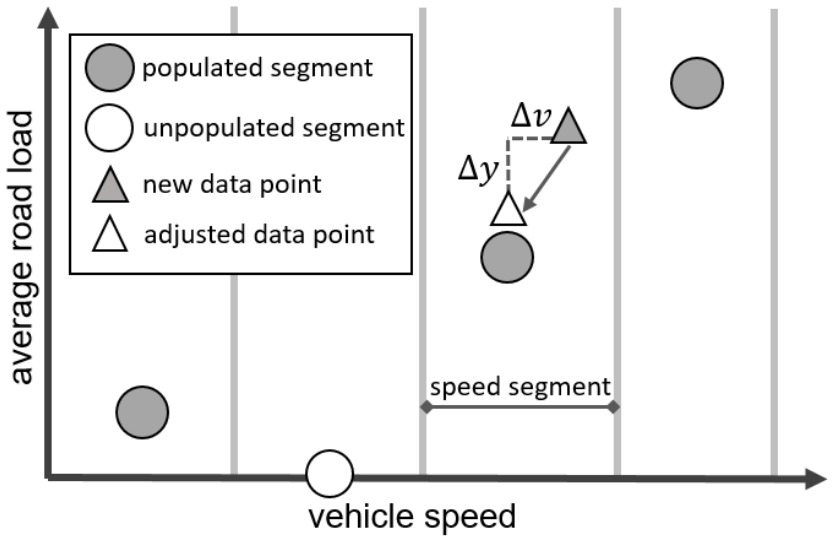

Fig.4.4 Schematic illustration of the measurement update process

In step 5, the average road load $\bar{y}_i$ in the speed segment i is updated with the new road load y_i, using the recursive average method in equation (4.13) and (4.14). The advantage of using recursive averaging is that it does not require the storage of previous measurements.

$$\bar{y}_{i,k} = \frac{n_{i,k}-1}{n_{i,k}} \bar{y}_{i,k-1} + \frac{1}{n_{i,k}} y_{i,k} \qquad (4.13)$$

$$n_{i,k} = n_{i,k-1} + 1 \qquad (4.14)$$

4.2.4 Parameters Estimation

The Weighted Recursive Least Squares (WRLS) algorithm is proposed in this section. The algorithm is based on the RLS algorithm. However, the algorithm is performed on the average road load of the speed segments Y instead of the input data. The steps of the WRLS algorithm is shown in Alg.4.2.

In step 1, the algorithm determines whether to conduct the parameters estimation. The estimation is conducted at the end of a data extraction event (described in section 2.2), which is indicated by the previous data extraction criteria being satisfied, and the current data extract criteria being unsatisfied.

In step 2 to 7, the RLS algorithm is performed on the average road load of the speed segments Y. In step 3, the algorithm checks if a segment is populated by comparing the number of the measurements n_i. In step 4, the algorithm calculated the weighting factor for the speed segment using equation (4.15).

$$R_i = \frac{R}{n_i} \qquad (4.15)$$

The measurement variance of a speed segment R_i is proportional to the variance of an individual sample R and the inverse of the number of samples n_i. This is because the measurement in a speed segment is an average road load. The variance of a sample average is proportional to the inverse of the number of samples, based on the *Central Limit Theorem* [88]. The number of samples n_i serves as a weighting factor. Segments with more measurements will have smaller variance R_i, and therefore, greater impact on the result.

In step 5, the average road load in the speed segments are passed to the RLS algorithm to estimate the vehicle parameters. The least square method is suitable for a system that is linear in parameters as in equation (4.6). It finds the parameters which minimizes the sum of squared error. Directly solving the problem is computationally intensive. And thus, the RLS method is used to update the parameters by iteration [89]. The steps of the RLS algorithm is shown as follows:

$$K_i = P_{i-1}\phi_i^T(\phi_i P_{i-1}\phi_i^T + R_i)^{-1} \qquad (4.16)$$

$$\hat{\theta}_i = \hat{\theta}_{i-1} + K_i\left(y_i - \phi_i\,\hat{\theta}_{i-1}\right) \qquad (4.17)$$

$$P_i = (I - K_i\phi_i)P_{i-1} \qquad (4.18)$$

Where $\hat{\theta}$ are the vehicle parameters including rolling resistance and aerodynamic drag coefficient as shown equation (4.10). The measurement variance R_i is calculated in

equation (4.15). ϕ is the input variables as in equation (4.9). The input speed corresponds to the middle speed of the segment speed. The estimator gain K, error covariance P, and vehicle parameters $\hat{\theta}$ are solved iteratively using the average road load stored in each speed segments.

4.3 Experimental Method

4.3.1 Data Acquisition

Real-world driving data was collected and to be used in a simulation environment to evaluate the proposed algorithm. The signals from the CAN bus were recorded with a 50 Hz sampling rate, including vehicle speed, engine torque, engine speed, longitudinal and lateral acceleration, brake on/off signal, and road grade measurement. The vehicle speed, engine speed, and engine torque can be found in the CAN bus J1939 standard [90]. The engine speed signal has high accuracy. However, the engine torque signal is less reliable, particularly at low engine load [91]. Auxiliary loads, such as the load of the fan, alternator, and compressor, are also considered when calculating the net engine output torque. The road grade is measured with an onboard inclinometer and has been processed with internal filtering. The vehicle mass can be estimated using the methods in[17][18]. In this section, the actual vehicle mass is used as a known variable to exclude the error brought in by the mass estimation.

The vehicle used for data acquisition was a medium size truck as shown in Fig.4.5. The model and configuration of the vehicle are detailed in Table 4.1. A typical value of rolling resistance coefficient C_r is between 0.006 and 0.013, depending on the

property of tire and the road pavement [92]. The typical value of aerodynamic drag coefficient C_d for the test vehicle is between 0.6 to 1.0 [93]. Accounting the vehicle frontal area and air density, the lumped coefficient C_{dL} is between 2.4 to 4. A coast-down test was conducted, according to the SAE 2263 standard [94], to measure the actual values of C_{dL} and C_r. The result suggests the value of C_{dL} and C_r of the vehicle is 2.62 and 0.0069, respectively.

Fig.4.5 Picture of the vehicle used for data acquisition

Table.4.1 Model and configuration of the testing vehicle

Vehicle make/ Model/ Year	Freightliner / M2-106/ 2011
Height × Width	2.90 m × 2.44 m
Front tires make/ Model	Goodyear/ G662 RSA
Front tires size	295/75 R22.5 G

Rear tires make/ Model	Goodyear/ G305 LH2
Rear tires size	295/75 R22.5 G
Vehicle weight (low/medium/high)	~8 ton/ ~12 ton/ ~14 ton
Estimated CdL	2.62
Estimated Cr	0.0069

The driving cycle serves to imitate typical daily driving. Each test was about 30 minutes long. The vehicle was operated for half an hour before each test to warm up the engine and tires. The test was repeated using low, medium, and high cargo weight. It is aimed to evaluate the robustness of the algorithm under different vehicle weight.

4.3.2 Comparison between WRLS and RLS

The real-world driving data was used to test the algorithm in a simulation environment. The estimation result of WRLS and RLS are compared in two situations: the city driving cycle with a small variation in speed, and a city and highway combined driving cycle with a large variation in speed. The same input signal and initial condition are used in the process.

The estimation results of the two algorithms using the 14-ton vehicle under the city cycle are shown in Fig.4.6. The cycle is repeated four times for the estimation results to converge. In the city driving cycle, only a few segments at low speeds have been populated, as shown in Fig.4.7. The estimation result of the RLS algorithm has a high error and fails to converge. In contract, the result of the WRLS algorithm is more robust.

This is because RLS algorithm is highly sensitive to the measurement error when vehicle speed has small variation. On the other hand, the WRLS algorithm can still produce robust results based on the prior information, when only a small number of the segments are available.

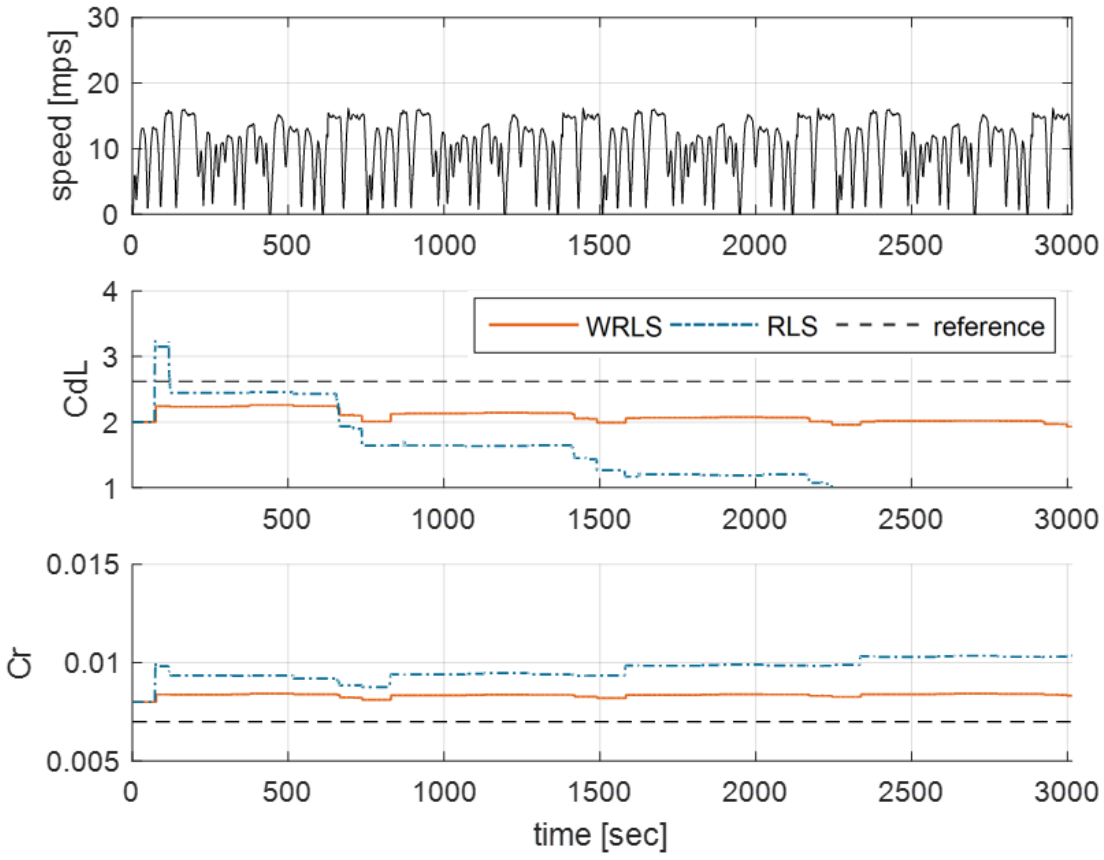

Fig .4.6 Parameters estimation results of the city driving cycle. Top: speed profile; Middle: lumped aerodynamic drag coefficient , Bottom rolling resistance coefficient.

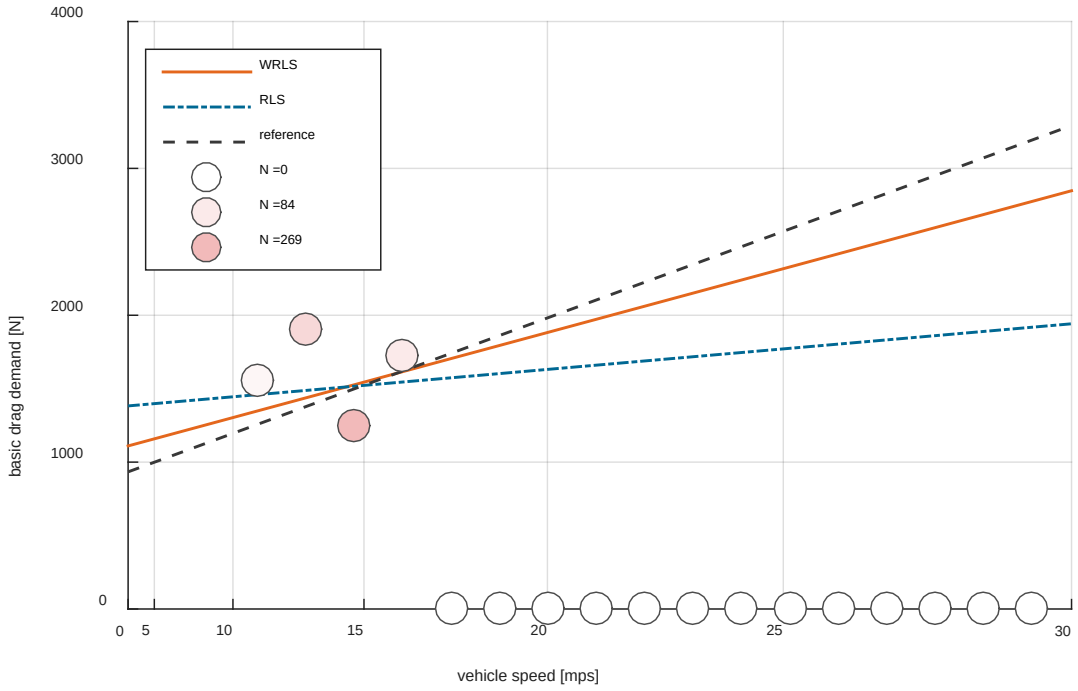

Fig.4.7 The speed segment results of the city driving cycle

The estimation results of the 14-ton vehicle under the combined city and highway cycle are shown in Fig.4.8. The cycle is repeated two times for the estimation results to converge. In the combined city and highway cycle, a wide variety of speed segments have been populated, as shown in Fig.4.9. The final estimation results of the two algorithms are similar. However, in the initial stage, the estimation of RLS is less reliable. This is because the data are from a narrow range of vehicle speed in the initial stage, which make the estimator more sensitive to the input error. After the data from higher speed being obtained, the RLS and WRLS algorithm both converge close to the actual value. The results of WRLS algorithm is 2.56 (-2.3% error) in estimating

aerodynamic drag coefficient and 0.0074 (7.2%) in estimating rolling resistance coefficient.

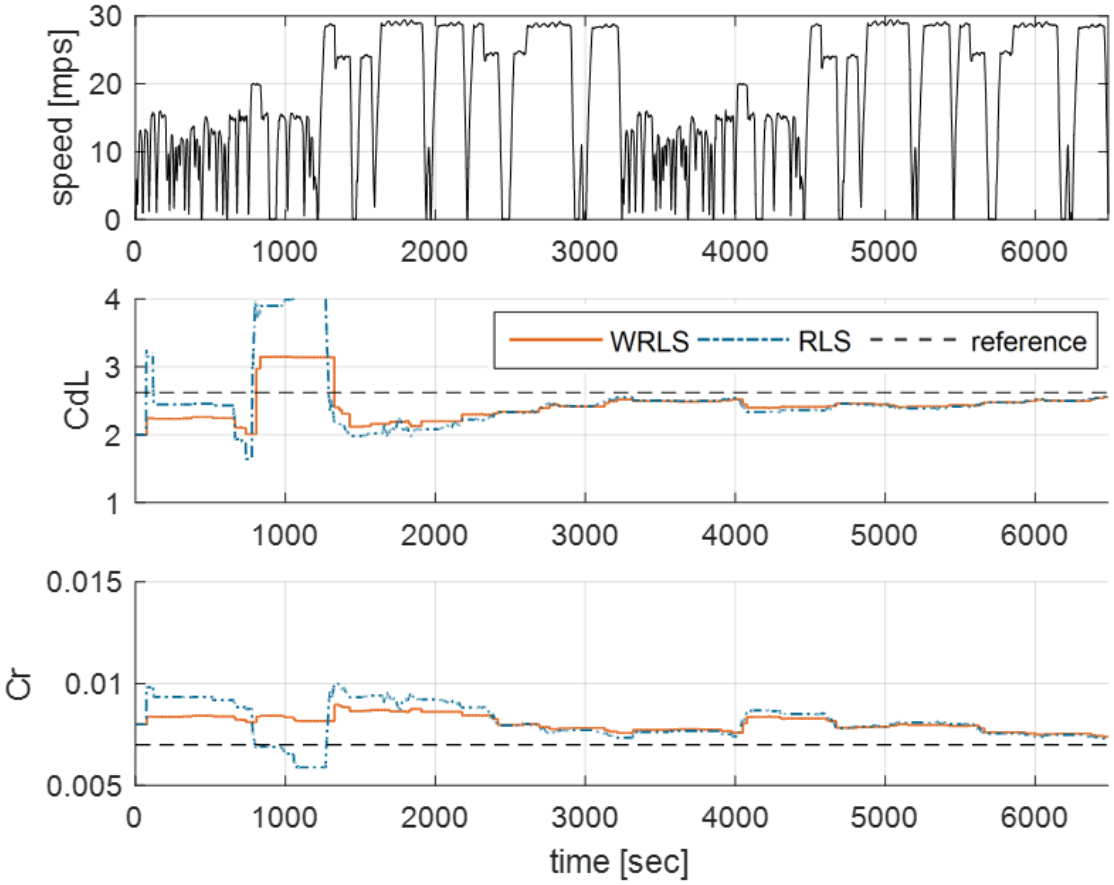

Fig.4.8 Results of a city driving cycle parameters estimation. Top: speed profile; Middle: lumped aerodynamic drag coefficient , Bottom rolling resistance coefficient.

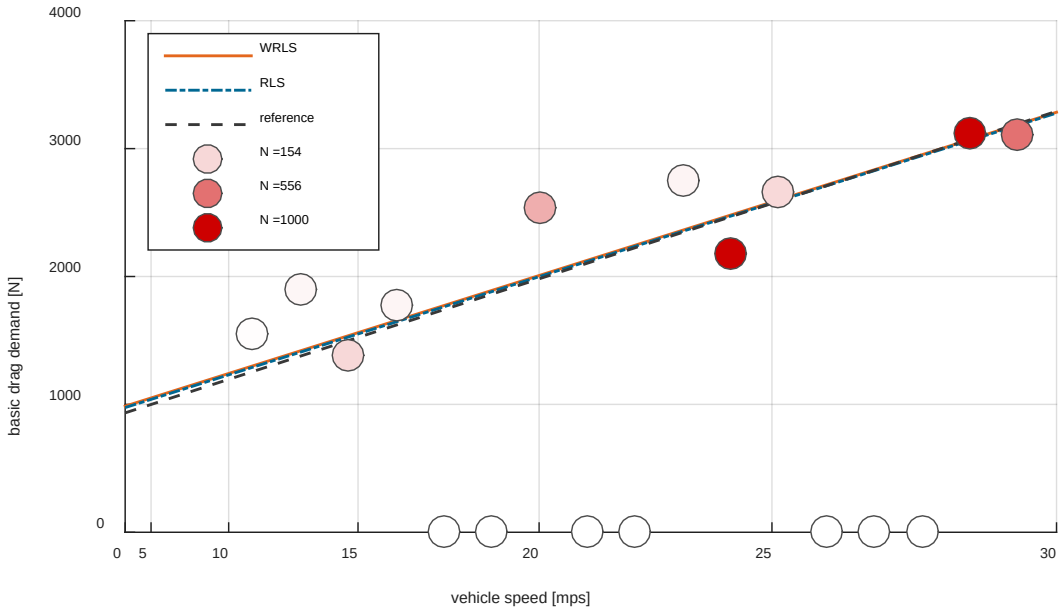

Fig.4.9 The speed segment result of the combined city and highway driving cycle

4.3.3 Impact of Vehicle Weight

In this section, the WRLS algorithm was tested to evaluate the impact of vehicle weight. The same vehicle was used with weight adjusted by the payload. The combined city and highway cycle was used. The final estimation results are shown in Table 4.2.

Table 4.2 Result of WRLS at different vehicle weight

	High (~14 ton)	Medium (~12 ton)	Low (~8 ton)
CdL (2.62)	2.56	2.63	2.55
CdL % error	-2.3%	0.4%	2.7%

Cr (0.0069)	0.0074	0.0080	0.0085
Cr % error	7.2%	15.9%	23.2%

The estimation results from the three different vehicle weights were similar, which shown the WRLS algorithm is robust under different vehicle weight. The algorithm achieves a high accuracy in estimating lumped aerodynamic drag coefficient (less than 5 percent error). However, the result of rolling resistance coefficient is less accurate (less than 25 percent error). One explanation for the rolling resistance being less accurate is that it accounts for less of the basic road load than the aerodynamic drag at high speed, and therefore, it is more sensitive to the measurement error. Another reason is that the actual rolling resistance in the real-world driving test may be higher than the reference value. This is because the rolling resistance increases with the vehicle speed. As most of the data in the test were obtained during the highway driving, the average rolling resistance in the real-world driving test tends to be higher than the reference value obtained in the coast down test.

4.4 Discussion

The memory and computational cost of the algorithm will be discussed in this section. The memory cost of the algorithm is $O(m)$, where m is the number of segments to discretize the speed. The memory cost does not depend on the number of samples

because the algorithm only stores the average basic road load for each speed segments. More generally, the memory cost for discretizing the input space is $O(m^i)$, where i is the number of dimension of the input space, m is the number of segments in each dimension. The memory cost grows exponentially as the input dimension increases. However, in the problem of estimating rolling resistance and aerodynamic drag coefficient the dimension of the input space is one, because only the vehicle speed is needed to be discretized.

The computational cost of the algorithm is $O(n)$, where n is the number of the samples. The computational cost grows linearly with the number of samples when calculating the basic road load and updating the speed segments. However, the parameters estimation steps are conducted on the average road load of the speed segments. And therefore it does not depend on the number of samples. The algorithm is efficient in memory and computation and thus is suitable for implementation in the powertrain control units.

4.5 Conclusion

Estimating the rolling resistance and aerodynamic drag allows the powertrain controllers to predict the road load and adjust to the wide variety of configurations in a fleet of commercial vehicles. Simultaneous estimating the two parameters often requires a wide variation of vehicle speed, which can be difficult to occur in real-world driving. To overcome this limitation, the Weighted Recursive Least Squares (WRLS) algorithm was proposed in this section, which stores the average road load at different speed segments and weights the measurements by the number of samples. The WRLS

algorithm was tested using the Real-world driving data and shown a more robust result than the RLS algorithm under different driving cycles, and a high accuracy in estimating aerodynamic drag coefficient under different vehicle weight.

In the future work, the parameters in the estimator can be better calibrated by studying the statistics of the measurement error. The estimator can be implemented in powertrain control units to adapt the control scheme with different vehicle configurations and improve the vehicle fuel efficiency.

CHAPTER FIVE

DRIVER BEHAVIOR CLASSIFICATION

5.1 Introduction

A vehicle's real-world fuel consumption largely depends on the driver behavior. Aggressive driving behavior (e.g. abruptly accelerating and braking) can significantly increase fuel consumption by up to 20-30 percent [13]. Characterizing the ecological driving (eco-driving) behavior has been investigated in the recent decades, both for enhancing the awareness of human driver [37][38] and in the quest to automatically adjusting the powertrain control schemes[95][96].

The driver behavior classification typically proceeds in two stages: feature extraction and classification. The feature extraction stage is considered more challenging. Previous studies have used features based on the statistical and frequency analysis of the driving data. However, the robustness of the schemes across different vehicles and driving cycles still leaves room for improvement.

In this chapter, a microtrip-based driver scoring algorithm is proposed which uses the signals from the CAN bus. To further improve the computational and memory efficiency, the algorithm converts the time-series driving data into events represented by symbolic data. The algorithm was tested with real-world driving data from medium and heavy-duty trucks. A high classification accuracy across different vehicles and driving cycles was achieved.

5.2 Driver Scoring Algorithm

The driver score algorithm receives the driving data from the vehicle CAN bus as the input and produces a driver score. The algorithm comprises of five steps, as shown in Fig 5.1.

Step 1: the algorithm converts the time-series driving data into events represented by the symbolic data.

Step 2: the algorithm determines the duration of a classification by identifying microtrips, which are small segments of the speed profile bounded by large acceleration and deceleration.

Step 3: the algorithm extracts features from the microtrip.

Step 4: the algorithm selected a classifier for the feature vector, based on the average speed of the microtrip and produces a score as the classification result.

Step 5: the algorithm aggregates the microtrips scores and computes the average value as the driver score.

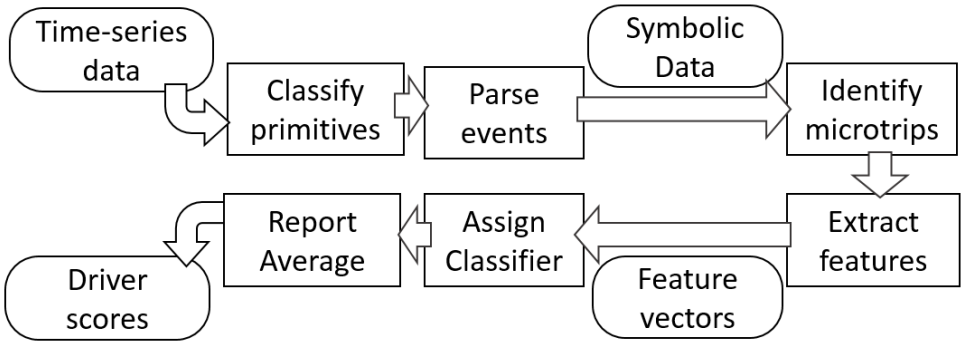

Fig.5.1 The flow diagram of the driver behavior classification process

In this chapter, we shall assume the data is obtained in the naturalistic driving environments, in which the stops, turns, and traffic lights will create the increases and decreases in the vehicle speed.

Our approach falls into the realm of supervised learning. Hence, it requires the data to be labeled. While a large amount of real-world driving data has been collected [97], the data labeled by driver aggressiveness is not readily available. The experimental setup will be detailed in section 5.4. Finally, the driver score provided by the algorithm will be validated by real-world fuel consumption.

5.2.1 Representing the Driving Data as Events

A promising approach to extracting features from the time-series data is to convert them into symbolic data, and then find features using symbolic pattern recognition [98], [99]. The study by Verwer et al. [100] has investigated the problem by converting the data into driving events (e.g. accelerating, decelerating and cornering).

We propose a new scheme to convert the time-series data into driving events, which are represented as discrete symbolic data. The algorithm is detailed in Alg.5.1 in the Appendix. The time-series driving data at any time step are represented as a 3-tuple:

$$(v, a_c, t_p) \qquad (5.1)$$

Where v is the vehicle speed, a_c is the acceleration and t_p is the throttle position. The acceleration signal has been passed through a low-pass filter to reduce the noise.

A. Primitive Assigning

The next step is to assign the 3-tuple (v, a_c, t_p) a nominal value, which is referred as the primitive or $\boldsymbol{p}$. In particular, five primitives are defined: accelerating (**a**), decelerating (**d**), sustain (**s**), coasting (**c**), idling (**i**).

$$\boldsymbol{p} \in \{\mathbf{a}, \mathbf{d}, \mathbf{c}, \mathbf{s}, \mathbf{i}\} \qquad (5.2)$$

The classification rules are defined as follows:

$$\boldsymbol{p} = \begin{cases} \mathbf{a} \text{ if } (\, v > 0\,) \wedge (a_c \geq \mathrm{a_{cU}}\,) \\ \mathbf{d} \text{ if } (\ v > 0) \wedge (a_c \leq \mathrm{a_{cL}}) \\ \mathbf{c} \text{ if } (v > 0)\ \wedge (\mathrm{a_{cL}} < a_c < \mathrm{a_{cU}})\ \wedge (t_p <\ \mathrm{t_{pL}}) \\ \mathbf{s} \text{ if } (v > 0)\ \wedge (\mathrm{a_{cL}} < a_c < \mathrm{a_{cU}})\ \wedge (t_p \geq\ \mathrm{t_{pL}}) \\ \mathbf{i} \text{ if } (v = 0) \wedge (t_p =\ 0) \end{cases} \qquad (5.3)$$

If a_c–acceleration exceeds an upper bound $\mathrm{a_{cU}}$, the event would be considered as accelerating (**a)**. Similarly, if a_c falls below a lower bound $\mathrm{a_{cL}}$, the event would be considered as decelerating (**d)**; if a_c is in between $\mathrm{a_{cU}}$ and $\mathrm{a_{cL}}$, the event will be considered as either sustain (**s)** or coasting (**c)**, which will be further distinguished by t_p–throttle position. And finally, if v–vehicle speed and t_p–throttle position are 0, the event would be classified as idling. An illustration of the rule-based primitive classification is shown in Fig.5.2.

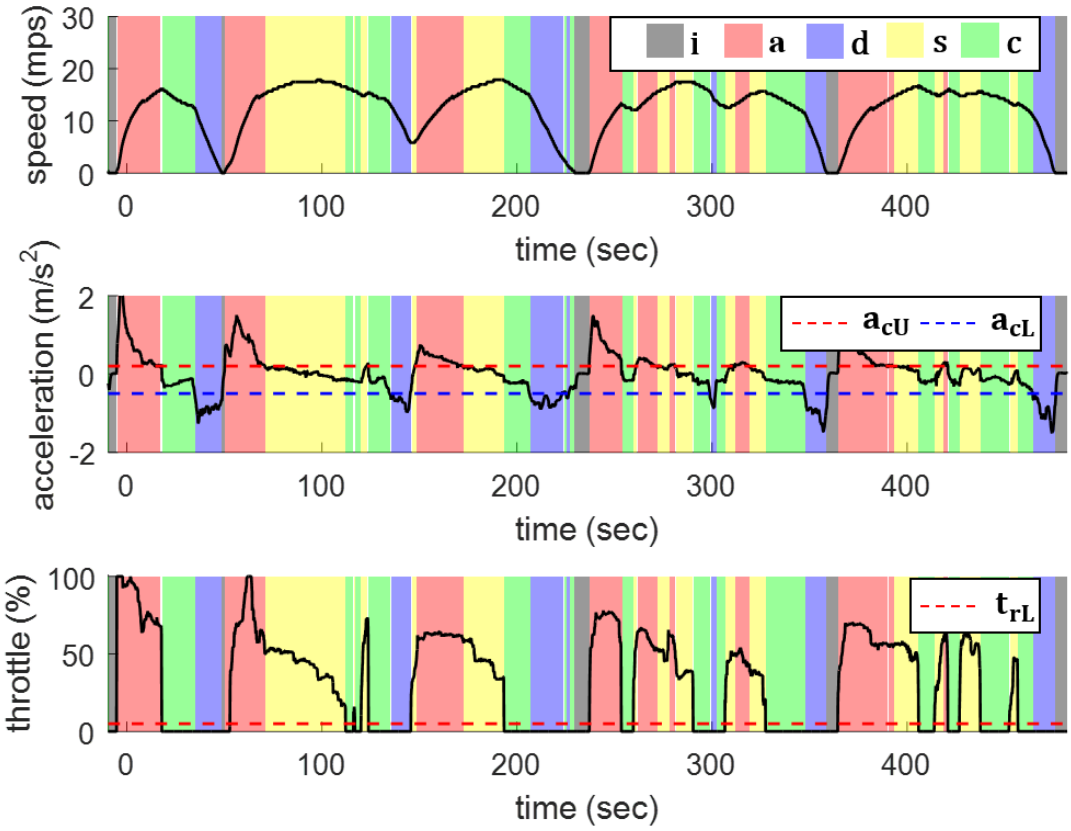

Fig.5.2 Illustration of the primitive classification

B. Event Parsing

Once a primitive $\boldsymbol{p}$ has been assigned at each time step, the next step is to group the adjacent primitives with the same value into one event. An event is defined as a 4-tuple including, *p*–primitive, v_0–starting speed, v_1–end speed, and *t*–duration, as shown in:

$$(\boldsymbol{p}, v_0, v_1, t) \qquad (5.4)$$

where, $\boldsymbol{p}$ takes nominal values; v_0, v_1,and t take numerical values. If the current primitive is different from the previous one, the algorithm ends the previous event and start a new event. In the case when a primitive sequence is too short, the event will be discarded. Fig.5.3 shows an illustration of the event parsing process.

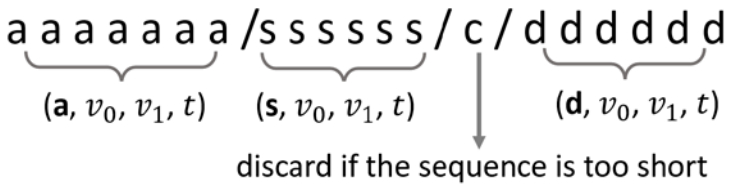

Fig.5.3 The illustration of the event parsing process

After the event parsing process, the time-series data have been converted to a sequence of events, which consists of both nominal value and numerical value. A piecewise linear approximation of the driving cycle can be reconstructed from the sequence as shown in Fig.5.4.

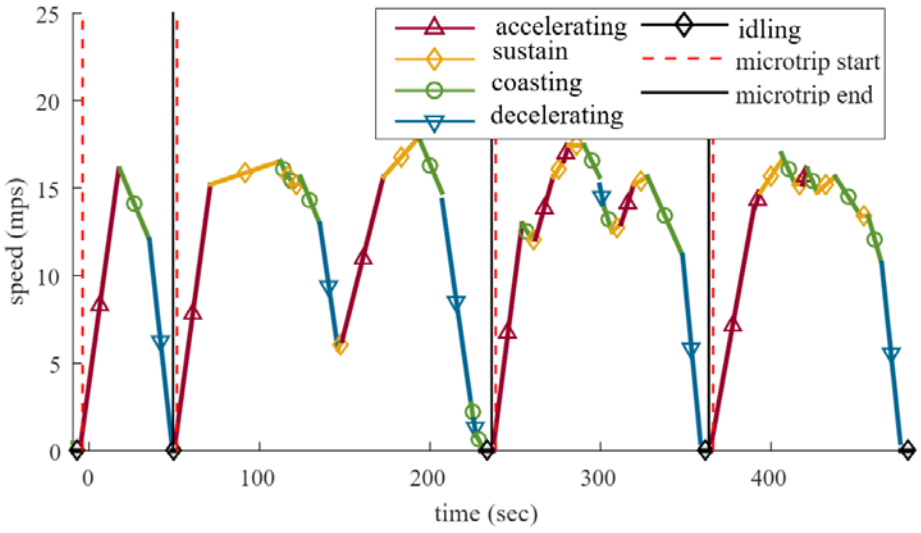

Fig.5.4 Piecewise linear approximation of a driving cycle

5.2.2 Microtrip Identification

The previous literature has primarily based the classification on an entire driving cycle. In contrast, the proposed algorithm bases the classification on the microtrips, and each microtrip will be characterized by a feature vector. The real-world driving often naturally consist of rises and falls in vehicle speed due to the turns, stops, and traffic lights. The concept of microtrips was originally defined as the speed profile bounded by the idling events [101] in vehicle test environment. However, in real-world driving the vehicle speed does not necessarily decrease to zero. And therefore, a modification has been made as illustrated in Fig.5.5. The definition of microtrips is as follows:

(1) Microtrips start when a large accelerating event occurs at low speeds.

(2) Microtrips end when an idling event exceeds a time limit or when a new microtrip starts.

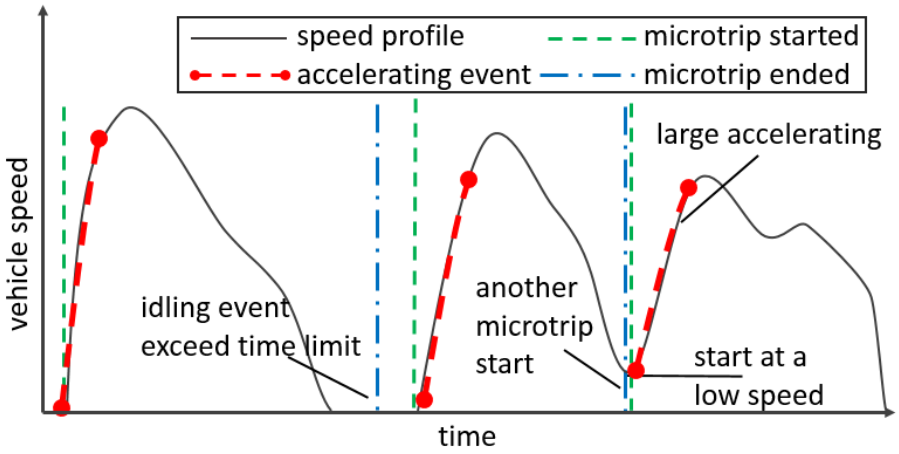

Fig.5.5 illustration of the microtrip identification

The identification of microtrips is realized through a finite state machine as shown in Fig.5.6. The algorithm is detailed in Alg.5.2 in the Appendix. An illustration the microtrip identification process is shown in Fig.5.6.

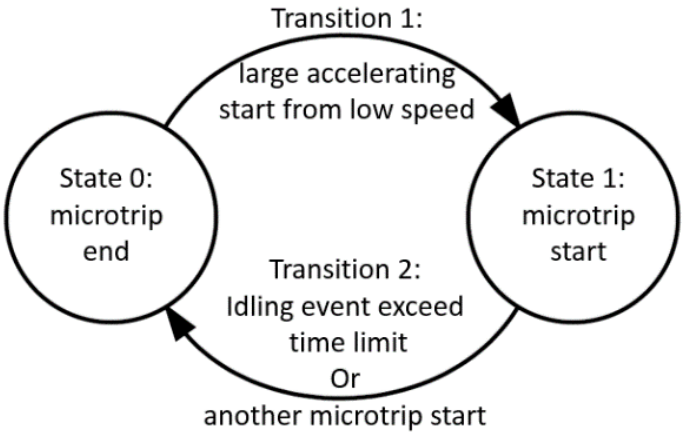

Fig.5.6 Finite state machine of the microtrip identification

5.2.3 Feature Selection

Feature selection is an important aspect of the driver behavior classification problem. Previous studies have used features based on statistic and the frequency content of the driving data. However, the features are often restricted to a certain vehicle and driving cycle. Our goal is to find features which are robust across the different vehicle and driving cycle.

The characteristics of the eco-driving behavior are subjective and ambiguous. According to the “golden rules” of eco-driving [102], it includes maintaining a steady speed, applying moderate acceleration and braking, and anticipating the further driving condition. Based on these general guidelines, five features are defined as follows.

Feature 1: deceleration level.

$$x_1 = \frac{1}{m}\sum_{i=1}^{m}\left(\frac{v_{0i}-v_{1i}}{t_i}\right) \forall i \in \{i|\, p_i = \mathbf{d}\,\} \qquad (5.5)$$

x_1 is defined as the mean acceleration in decelerating events **d**. The acceleration is approximated from start speed v_0, stop speed v_1 and the duration t_i of an event.

Feature 2: coasting time.

$$x_2 = \frac{1}{m}\sum_{i=1}^{m}(\, t_i) \quad \forall i \in \{\boldsymbol{p_i} = \mathbf{c} \wedge \boldsymbol{p_{i+1}} = \mathbf{d}\} \quad (5.6)$$

x_2 is defined as the mean duration of coasting events **c** before deceleration events **d** . $\boldsymbol{p_i}$ and $\boldsymbol{p_{i+1}}$ denote the current and the next event. The feature only considers the coasting events **c** before the decelerating events **d**. The coasting time before braking reflects the driver anticipation of the future traffic.

Feature 3: specific kinetic energy index.

$$x_3 = \frac{\sum_{i=1}^{i=m}(\, v_{1i}^2 - v_{0i}^2)}{\frac{1}{2}\sum(v_0+v_1)t} \quad \forall i \in \{\boldsymbol{p_i} = \boldsymbol{a} \vee \mathbf{s}\ , v_{1i} > v_{0i}\} (5.7)$$

x_3 is defined as the kinetic energy consumed per distance traveled and per unit mass. The denominator approximates the total travel distance. The numerator approximates the kinetic energy from the vehicle speed gain during the accelerating **a** and sustain **s** events. Aggressive drivers tend to accelerate the vehicles to higher speeds than necessary, and thus, result in higher kinetic energy. The mean value of the feature tends to decrease as the average speed increases, as has been shown in the study by Duran and Walkowicz [97], in which a similar kinetic energy metric has been defined.

Feature 4: acceleration level.

$$x_4 = \frac{1}{m}\sum_{i=1}^{i=m}\left(\frac{v_{0i}-v_{1i}}{t_i}\right) \forall i \in \{\boldsymbol{p_i} = \mathbf{a}\} \quad (5.8)$$

x_4 is defined as the mean acceleration during acceleration events **a**. Similar as in x_1, the acceleration is approximated from start speed v_0, stop speed $v_1$and the duration t of an event.

Feature 5: the portion of coasting.

$$x_5 = \frac{\sum_{i=1}^{n} t_i}{\sum t} \forall i \in \{\boldsymbol{p_i} = \mathbf{c}\} (5.9)$$

x_5 is defined as the portion of coasting event **c** in the entire duration of the microtrip. It reflects the driver's anticipation of the future traffic.

5.2.4 Classification Algorithm

Various algorithms can be found in the category of the supervised learning. The Logistic Regression algorithm [103] is chosen for the following reasons. First, the decision rules are explicit, and thus, the output can be easily traced back from the value of each feature. Secondly, the algorithm is computationally efficient for prediction, and therefore, is suitable to be implemented in real time.

The output of the classification is a continuous number, which presents the probability of whether the data belongs to a class or the other. The hypothesis function of the logistic regression is:

$$h_\theta(x) = g(\theta^T x) = \frac{1}{1+e^{-\theta^T x}} \quad (5.10)$$

Where, x is the feature vector, θ is the set of parameters, $\theta^T x$ is a linear combination of the features and parameters. g is the nonlinear sigmoid function, which maps $\theta^T x$ from $\mathbb{R}$ to [0, 1]. The cost of function of (10) is shown in (11). Following the common practice in logistic regression, a regulation term is added to prevent overfitting.

$$J(\theta) = -\frac{1}{m}\sum_{i=1}^{m}\left[y^{(i)}\log\left(h_\theta\left(x^{(i)}\right)\right) + \left(1-y^{(i)}\right)y^{(i)}\log\left(1-h_\theta\left(x^{(i)}\right)\right)\right] + \frac{\lambda}{2m}\sum_{j=1}^{n}\theta_j^2 \quad (5.11)$$

The last term $\frac{\lambda}{2m}\sum_{j=1}^{n}\theta_j^2$ is the regularization terms. It penalizes parameters with the large magnitude in order to prevent overfitting. λ is the regularization parameter. The equation (5.11) can be solved by several iteration methods. The Newton's method is used, which has the advantage of faster convergence comparing with the gradient descent method. The method uses the information of the second derivative or Hessian to change the step size at each iteration. The update rules for newton's method is:

$$\theta^{(t+1)} = \theta^{(t)} - H^{-1}\nabla_\theta J \quad (5.12)$$

A detailed description of the algorithm can be found in [103].

5.3.6 Speed Segmentation

The value of features tends to vary on average vehicle speed, which could poses a challenge for linear classifier. For example, the distribution of Feature 3 specific kinetic energy index at different average speed is shown in Fig. 5.7. The value tends to be higher at the lower speed, because at the lower speed a higher portion of energy is consumed to

accelerating the vehicle. To further enhance the classification accuracy, the microtrips are grouped into segments based on the average speed. Thus, the microtrips in the same segment are more comparable. Each segment has a unique classifier, which is trained with data only from that segment. During the predicting step, a classifier is selected based on which segment the current microtrip belongs to.

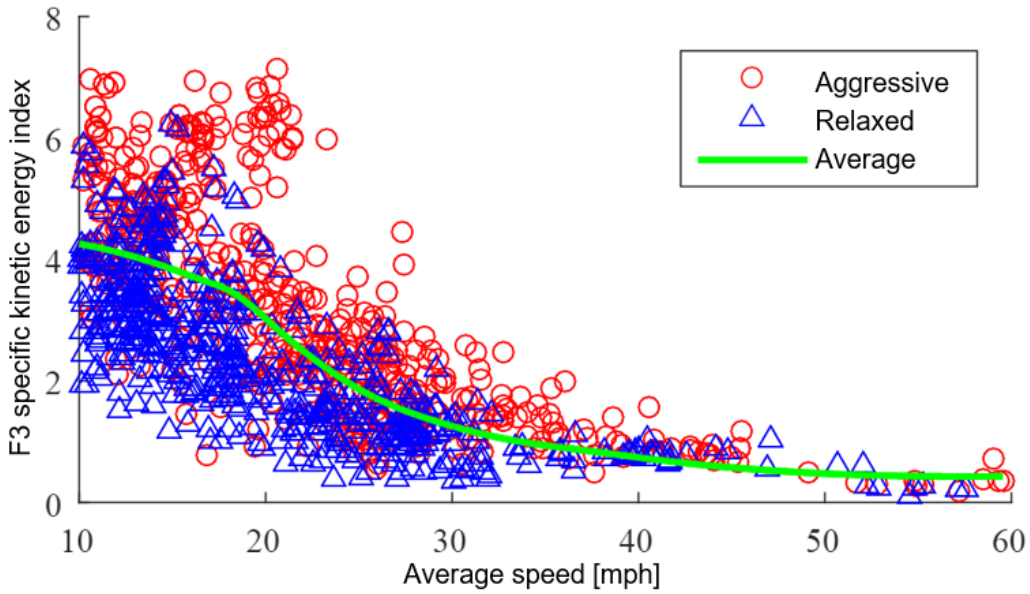

Fig. 5.7 Distribution of feature 3 specific kinetic energy index at different speed

A trade-off presents itself in choosing the range of the speed segments. If the range is too close, less training data will be left in each segment; one the other hand, if the range is too broad, the data in each segment will have a wide dispersion. As a general guidance, the speed range should be smaller when the values of the features change rapidly with the average microtrip speed. Four segments are chosen with the average speed ranges from 5 to 10 [m/s], 10 to 15 [m/s], 15 to 20 [m/s] and above 20 [m/s]. The

minimal average speed is 5 [m/s] to exclude the data at low speeds. The speed range of each segment is shown in Table 5.1.

Table 5.1 the range of discrete speed segments

Segment#	1	2	3	4
Speed range(mps)	5-10	10-15	15-20	20 up

5.3.7 Driver Score

In the previous steps, the Logistic Regression based classifiers classify each microtrips, and produce a microtrip score s, which indicates the probability of whether it belongs to the relaxed or aggressive driving.

In the next step, the algorithm aggregates the microtrip scores and computes the driver score S by averaging the scores of all micro-trips as show in (3) and Fig.5.8.

$$S = \bar{s} \qquad (5.13)$$

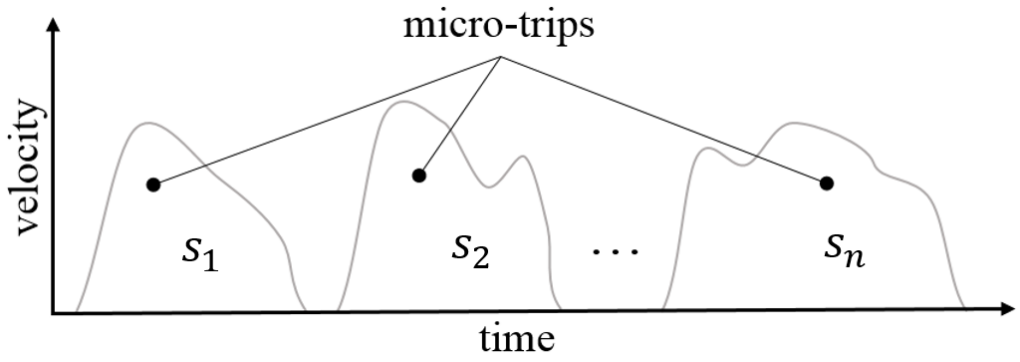

Fig.5.8 Schematic illustration of micro-trips

The driver scoring algorithm is shown in the Appendix as Alg.5.2. By using finite-state-machine and recursive average, the algorithm does not require logging the driving data which considerably reduces the memory overhead.

5.3 Experimental Results

5.3.1 Data Acquisition

The data acquisition process is described in this section. The experiment was conducted by the industry partner. The labeled data was obtained by the drivers imitating aggressive and relaxed driving behavior. Some details of the study are described as follows:

1) Sixteen drivers participated in the study to reduce the difference of the individual driving behavior.
2) Three vehicles were used to represent a variety of vehicle types including 2 medium-duty trucks and 1 heavy-duty truck with different weights. The weight of each vehicle is shown in Table 5.2.
3) Over twenty-six hours of driving data were recorded. The driving data was obtained from the vehicle CAN bus. The signal included vehicle speed, longitudinal acceleration, throttle position, fuel rate, and the GPS data. The sampling frequency was 10 Hz. The vehicle speed, longitudinal acceleration, throttle position are used as inputs to the algorithm. The fuel rate data is used to validate the driver score in reflecting the real-world fuel consumption. The GPS data is used to inspect the routes visually and is not used as inputs to the algorithm.

Table 5.2 Test vehicle type and weight

Vehicle#	A	B	D
Vehicle type	medium-duty truck	medium-duty truck	heavy-duty truck
Vehicle mass (kg)	8700	13000	20500

Table 5.3 Summary of data acquisition settings

# Vehicle	3
# Driver	16
Total driving minute	1554
Signals	Vehicle speed, Longitudinal accelerating, Throttle position, Fuel rate, GPS

General guidelines were given to the driver to mimic a particular driving behavior. The guidelines for the relaxed behavior includes:

1) Anticipate traffic flow and road grade; use vehicle momentum to reduce braking.
2) Follow the traffic flow up to the speed limit; the driver should not deliberately attempt to lower the vehicle speed to achieve better fuel economy.

The guidelines for the aggressive driving behavior includes:

1) Exercise unnecessary, perpetual and sharp acceleration.

2) Display bad anticipation of future traffic and increase the use of brakes.

The majority of the driving data was collected in a city driving condition with the presence of moderate traffic. To represent different driving cycles, the data of two additional traffic conditions were collected. One is from the heavy-city-driving condition, which consists of a high portion of start-stop traffic. The other is the suburban-driving condition, which consists of a more smooth traffic flow, and a high portion of driving at higher speeds.

The number of trips from the aggressive and relaxed driver is roughly equal. The summary of the amount of data collected grouped by vehicle and speed segment is shown in Table. 5.4. The table shows both the number of microtrips and the driving time in minutes. The higher speed segments have fewer microtrips because the duration of the individual microtrips is longer. Most of the data are collected using vehicle A. The additional vehicles were used with more emphasis on testing the algorithm's robustness across different vehicle types.

Table 5.4 The amount of data collected grouped by vehicle types and speed segments

Speed [mps]	A[a]/12[b]	B/4	C/4
5-10	370[c] (270)[d]	184 (99)	26 (30)
10-15	283 (587)	44 (48)	48 (89)
15-20	50 (145)	11 (20)	12 (39)
20 up	28 (101)	8 (28)	9 (98)

a: vehicle type, b: the number of driver, c: the number of microtrip, d: driving time in minute.

5.3.2 The Value of Features

The proposed algorithm was tested in a simulation environment using the real-world driving data. The features are normalized through the min-max normalization, and thus the values range from 0 to 1. The min-max normalization is described as:

$$x_i^* = \frac{x_i - x_{\min}}{x_{\max} - x_{\min}} \qquad (5.14)$$

Where, x_i^* is the normalized feature value, x_i is the original feature value, $x_{\max}$ and $x_{\min}$ are the maximum and minimum value of the feature.

The mean value of the features grouped by speed segments and vehicle types are shown in Fig.5.9. The filled the marker, and unfilled marker indicates the aggressive and relaxed driver respectively. The mean value of the total dataset is shown as the dashed line. Aggressive drivers tend to have higher values in x_1, x_3, x_4 (brake level, kinetic energy index, and acceleration level) and lower values in x_2, x_5 (coasting time, and coasting portion). The values of x_1 and x_5 (deceleration level, and the portion of coasting) are mostly constant across different speed segments. However,x_3, x_4 (specific kinetic energy, and acceleration level) tend to decrease as the segment speed increase. x_2 (coasting time) tends to increase as the segment speed increases.

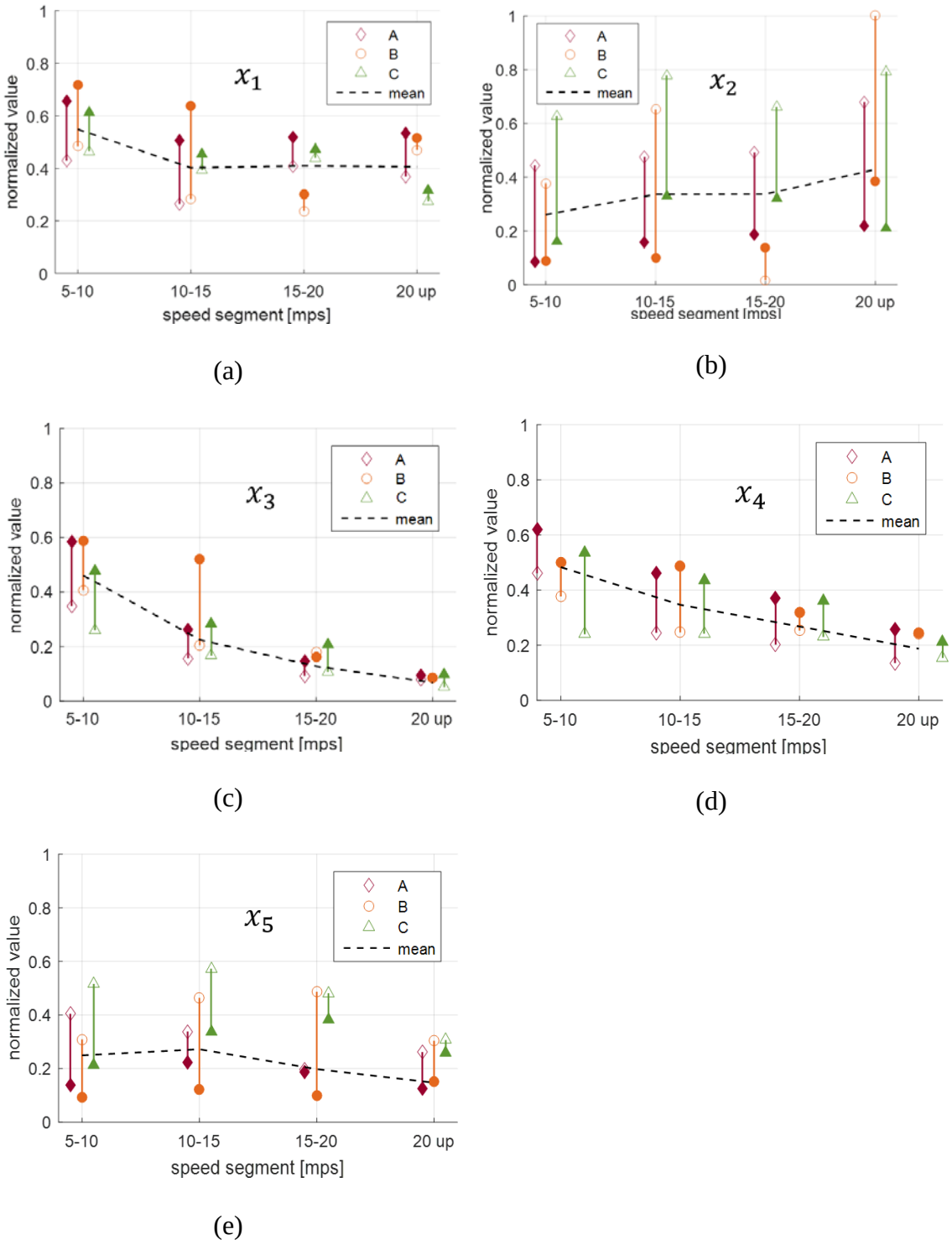

Fig.5.9 The mean value of features at various speed segment (a) x_1 deceleration level (b) x_2 coasting time (c) x_3 specific kinetic energy index (d) x_4 acceleration level (e) x_5

portion of coasting event. The filled marker indicates aggressive driver; the unfilled marker indicate relaxed driver; dashed line indicates the mean value of all the data at certain speed segment.

5.3.3 Principal Component Analysis

The Principal Component Analysis (PCA) is conducted to evaluate the feature with the largest variance. PCA converts the features into linearly uncorrelated variables (principal components). The principal components of the data are shown in 5.18.

$$M = \begin{bmatrix} -0.46 & 0.45 & 0.64 & 0.40 & -0.080 \\ 0.63 & 0.61 & 0.27 & -0.40 & -0.045 \\ -0.42 & 0.36 & -0.24 & -0.36 & 0.71 \\ -0.34 & 0.40 & -0.49 & -0.19 & -0.67 \\ 0.31 & 0.38 & -0.46 & 0.71 & 0.20 \end{bmatrix} \quad (5.15)$$

Each column response to each principal components, which are in the order of decreasing variance from left to right. Each row contains the coefficient of each feature for each principal component.

From the 1st principal component (1st column), x_2- coasting time has the large coefficient, it has a positive correlation with x_5-coast portion and negative correlation with x_1-deceleration level, x_3-kinetic energy,x_4-brake level.

The variance explanation ratio with the number of principal components is shown in Fig. 5.10. The first two principal component explains 86 percent of the variance. By reducing the data dimension to two, we can visualize the data as shown in 5.10.

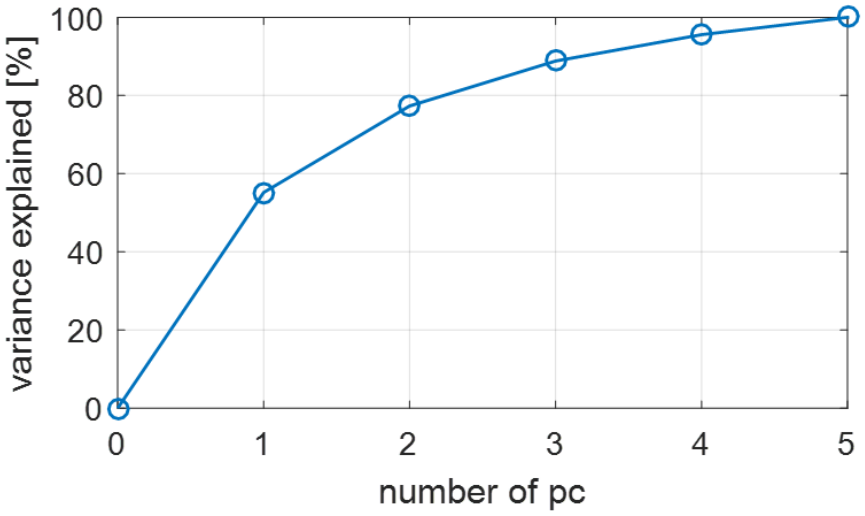

Fig.5.10 Variance explanation ratio of the principal component.

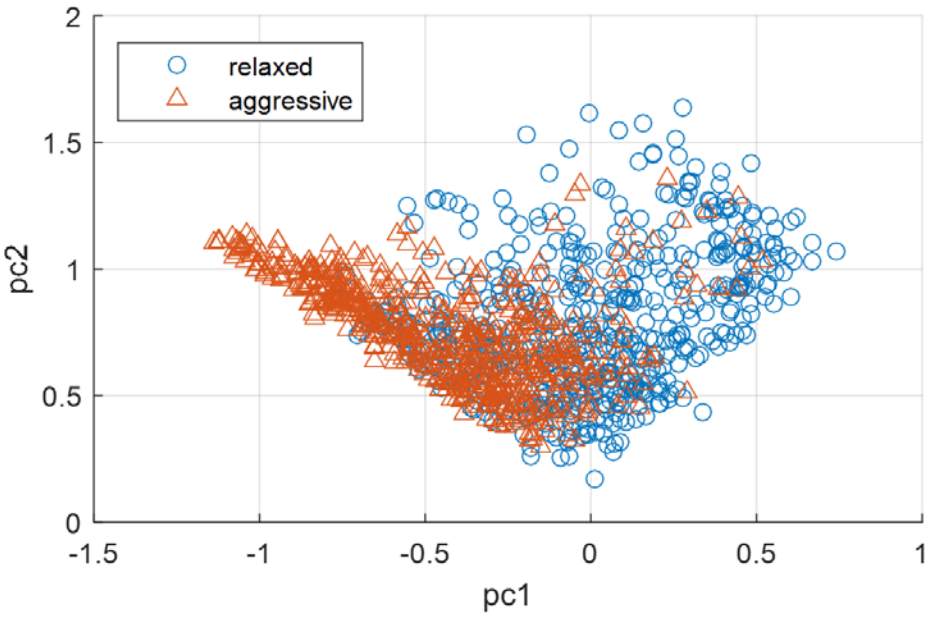

Fig.5.11 Visualization of the data on the first two principal components.

In Fig. 5.11, we can observe the 1st principal component (x-axis) is the most predictive. The data from relaxed drivers tend to locate toward the right, and the aggressive driver tend to locate toward the left.

5.3.4 Classification Results

The classification error was used as the performance metric, which is defined as the ratio of the number of misclassified data and the total number of data:

$$e = \frac{1}{n}\sum_{i=0}^{n} 1(\hat{y}_i \neq y_i) \quad (5.21)$$

The practice of 5-fold cross-validation was followed. The data from each vehicle type was divided into 5 folds. 1 fold was used as the test set, and the rest were used as training set, the process was repeated for each fold, and the average error rate was reported. The regularization parameter λ was determined through the grid search, which exhaustively examined the parameter from 0.01 to 0.2 with the increment of 0.01 and chose the parameter with the lowest classification error.

The final classification error using the 5 features is 17.3 percent. The confusion matrix in Table III shows the percentage of the true positive, false negative, false positive, and true negative categories. There are similar amounts of misclassifications in the category of false positive and false negative.

Table 5.5 Confusion matrix of the classification

		Predicted Class	
		True	False
Actual Class	True	37.4%	10.2%
	False	7.1%	45.3%

To evaluate the impact of the number of features on the classifier performance, every combination of 1 or more of the 5 features were tested. The same cross-validation procedure was taken. The regularization parameter λ was determined through grid search. The best results with 1 to 5 features are shown in Fig. 5.12.

x_2-coasting time is the most predictive parameter because it has the lowest error rate when using only one feature. The error rate plateaus after using 3 features. To simplify the computation, it is possible to just use 3 features (x_2-coasting time, x_4-acceleration level, and x_3- specific kinetic energy index) and obtain a similar level classification accuracy.

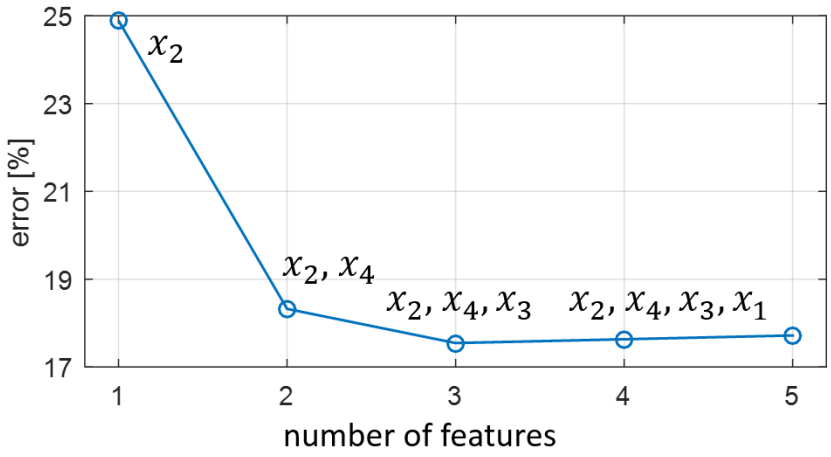

Fig.5.12. Classification error with the different number of features

5.3.5 Algorithms Comparison

The proposed algorithm uses speed segmentation to reduce the influence of vehicle speed on the features. To demonstrate the effectiveness of the speed segmentation, the proposed algorithm was compared with three additional algorithms, which do not employ the speed segmentation:

1) LR 1: Logistic Regression with speed segmentation (the proposed algorithm).
2) LR 2: Logistic Regression without speed segmentation, but use average microtrip speed as an additional feature.
3) LR 3: Logistic Regression with neither speed segmentation, nor using speed as a feature.
4) SVM: Support Vector Machine (RBF kernel)[103] without speed segmentation, but use average microtrip speed as an additional feature.

The same 5-fold cross-validation procedure was followed, and all the 5 features are used. The tuning parameter λ in logistic regression and c in SVM is determined using the grid search. The result is shown in Table. 5.6.

Table 5.6 Comparison between logistic regression and SVM

	Classification Error
Algorithm 1 (LR1)	17.3%
Algorithm 2 (LR2)	18.0%
Algorithm 3 (LR3)	21.2%
Algorithm 4 (SVM)	14.9%

The proposed algorithm using speed segmentation (LR 1) outperforms the algorithm using the average speed as an additional feature (LR 2). The algorithm, which uses neither the speed segmentation nor speed as a feature (LR 3), has the highest error rate.

The SVM algorithm has the lowest error rate. However, the model contains 344 support vectors, and it requires much greater memory and computation.

It can be observed that even with a more sophisticated algorithm like the SVM, the error rate is still around 15 percent. One explanation is that even though the data is labeled, it is not necessary that all the microtrips from the “aggressive” driver display the aggressiveness and vice versa. In some cases, the characteristic of the driver behavior can still be ambiguous. However, the uncertainty of the individual data can be reduced when considering many microtrips.

The classification error grouped by speed segment and vehicle types are shown in Fig.5.13. The error rate is similar across different vehicles. Vehicle A has slightly lower error rate because most of the training data are collected from this vehicle. The data is the most predictive in the speed segment 10-15 [m/s] because the algorithm has the lowest error rate in this region.

In summary, speed segmentation is effective for the simple classifier (e.g. logistic regression) to improve the classification accuracy. The algorithm is robust across different driving cycle and vehicle weights.

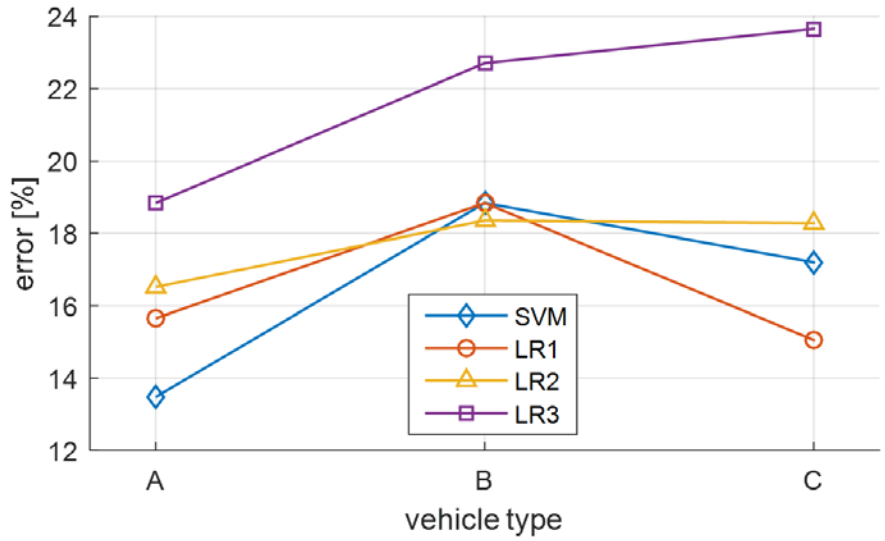

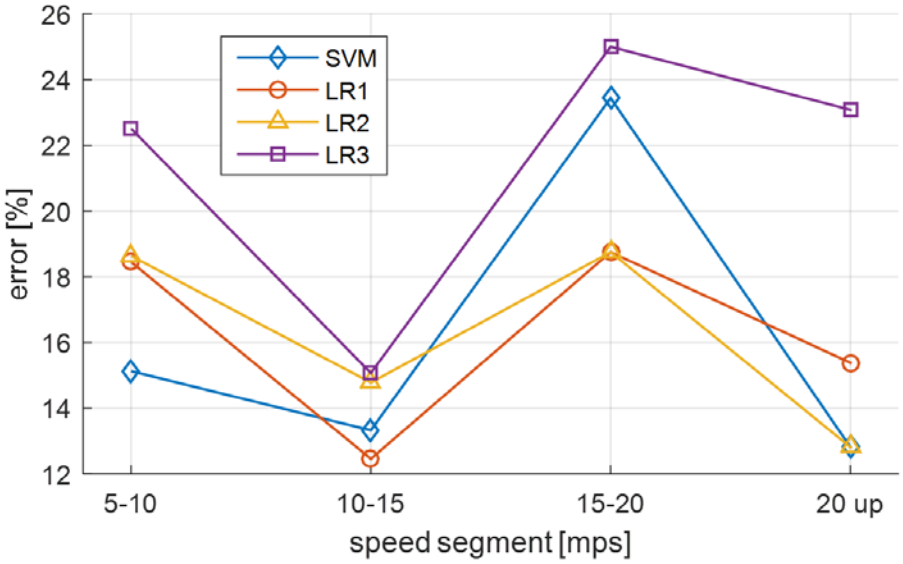

(b)

Fig.5.13 Classification accuracy (a) classification accuracy by speed segment (b) the classification accuracy by vehicle weight.

5.3.6 Validation with Fuel Consumption

To validate the driver score in reflecting the vehicle real-world fuel consumption, the correlation between the two variables was studied. Due to the fuel consumption is

only comparable to the same vehicle and driving cycle, 20 trips with the same vehicle (vehicle A) and route were chosen (10 each for the aggressive and relaxed driver). The parameters in the driver scoring algorithm were trained from the dataset in which the 20 trips were excluded. The vehicle's real-world fuel consumption was calculated from the fuel rate data, and normalized by its maximum and minimal value. The scatter plot of the two parameters is shown in Fig.5.14.

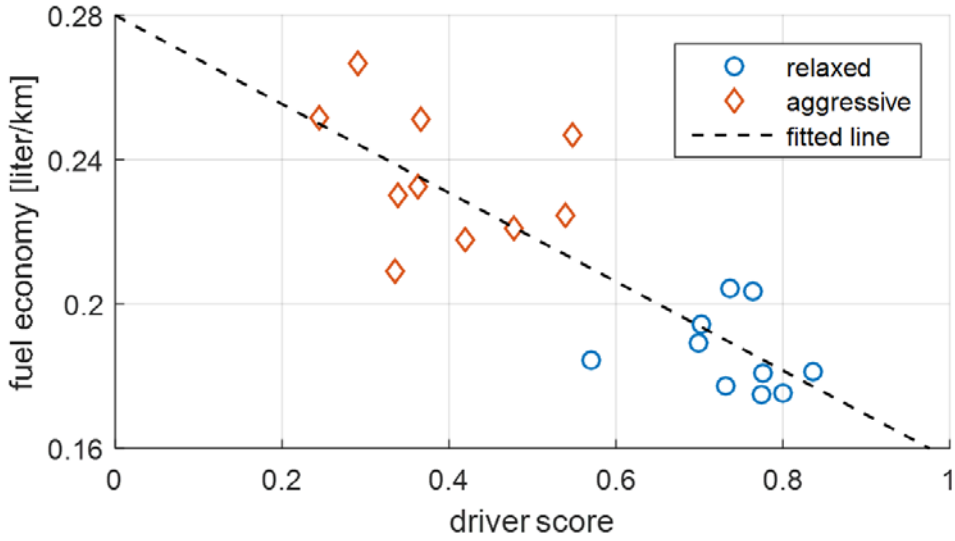

Fig.5.14 The correlation between driver score and vehicle fuel consumption

A high correlation between the driver score and vehicle fuel consumption can be observed. The dispersion of the real-world fuel consumption is affected by the driving behavior and the traffic conditions. Even though the same route was taken, the traffic flow and the occurrences of the traffic light can be different. Despite the effects of the traffic, a clear trend of the fuel consumption decreasing with the driver score can be observed.

The Pearson's correlation coefficient ρ is used to quantify the correlation relationship between the two parameters. The value of ρ ranges from -1 to 1. The closer the absolute value to 1, the stronger the correlation. The driver score and real-world fuel consumption have ρ= -0.84, which indicates a high correlation between the two parameters. And thus, the driver score is validated in reflecting the real-world fuel consumption.

5.4 Discussion

The memory and computational cost of the algorithm is discussed in this section. Regarding the computational cost, during the steps of converting the time-series data into feature vectors, the computation grows linearly with the number of sample or $O(n)$. In the predicting step, the algorithm uses the logistic regression, which is one of the fastest classification algorithms. Regarding the memory cost, the algorithm does not require logging on the driving data. By using the finite-state machine and recursive average algorithm the event parsing, feature extraction, and the microtrip identification process can be accomplished on-the-fly.

Based on the discussion above, the driver scoring algorithm has low memory and computational overhead. Therefore, it is suitable for real time implementation.

5.5 Conclusion

In summary, this section has proposed a driver scoring algorithm for classifying the eco-driving behavior. In contrast to the prior art, the algorithm bases the classification on the microtrips and converts the time-series data into symbolic data to facilitate feature extraction. Real-world driving data from a variety of driving cycles and vehicle types has been used to demonstrate the usefulness of the algorithm. The driver score produced by the algorithm has achieved a high classification accuracy in predicting the eco-driving behavior and has also shown a high correlation with the vehicle real-world fuel consumption.

In the future work, the performance of the algorithm can be further improved by collecting more data and through feature engineering.

CHAPTER SIX

ADAPTIVE SHIFT STRATEGY

6.1 Introduction

Commercial vehicles operating in a variety of vocations have different consciousness for fuel consumption and drivability. For example, delivery trucks might emphasize more on drivability to improve productivity. On the contrary, semi-trailer trucks can be more fuel conscious of reducing the fuel cost. As a result, the shift map often requires extensive calibration to different vocations. Using an adaptive shift strategy based on the driver behavior can reduce the initial transmission calibration effort and improve the real-world fuel consumption.

In this chapter, a new adaptive transmission shift strategy is proposed, which include an offline and an online stage, as shown in Fig.6.1. During the offline stage, the driving characteristics of different driver aggressiveness are studied, which will be used for generating the shift maps. Since obtaining the driving characteristics requires the vehicle to drive for an extended period, the previously developed driver score metrics is used as a proxy to match the driving characteristics in real time. During the online stage, after the driver score is obtained, the driving characteristics are reconstructed and used to generate the shift maps. Lastly, the objective metric of drivability is defined and the impact of different shift maps on drivability and fuel consumption is evaluated using the vehicle simulation.

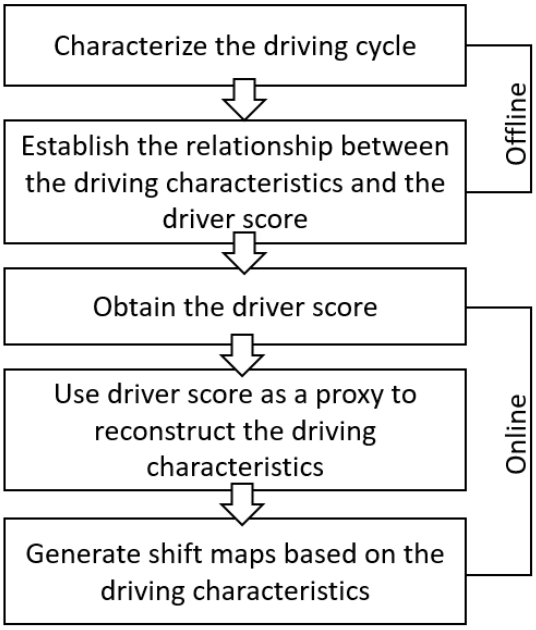

Fig.6.1 The adaptive shift strategy flow diagram

6.2 Generating the Shift Map

The process of the shift map generation is discussed in this section. The shift map is based on the percentage of the maximum torque demand and current vehicle speed. A typical shift line can be divided into three regions: the high torque region, the middle torque region, and the low torque region, as shown in Fig.6.2. The maximum and minimum vehicle speed of the shift line is denoted as $v_{\max}$, and $v_{\min}$ respectively.

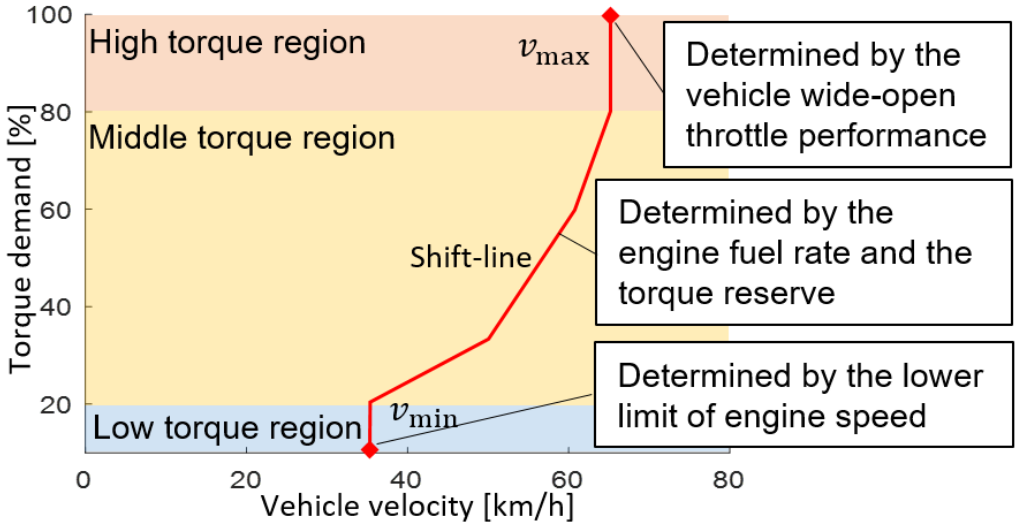

Fig.6.2 Regions of a typical shift line

6.2.1 Low Torque Region

The low torque region is defined as the interval between 0 and 20 percent of the torque demand. The minimal speed $v_{\min}$ is determined based on the lower limit of engine stall speed. The transmission must downshift if the engine speed falls below the minimal engine speed limit (1200 rpm).

6.2.2 High Torque Region

The high torque region is defined as the region above 80 percent of the torque demand. The maximum speed $v_{\max}$ determines the speed above which the transmission must upshift. $v_{\max}$ greatly affects the vehicle wide-open throttle performance. The maximum acceleration performance is obtained when a shift occurs at the intersection of the two maximum torque curves of the consecutive gears.

6.2.3 Middle Torque Region

The middle torque region is defined as the interval between 20 percent and 80 percent of the torque demand. The upshift speeds in this region are determined by minimizing the fuel consumption with the constraint to satisfy the torque reserve.

The torque reserve is commonly used to ensure drivability [104][105]. The torque reserve specifies the amount of additional torque that must be available at the current load. The torque reserve ensures the instantaneously available torque so that if the driver's torque demand increases, the transmission does not need to downshift to satisfy the driver demand, which ensures a smooth driving experience. If the instantaneously available torque is smaller than the required torque reserve, the upshifting is prohibited. As illustrated in the Fig.6.3, both operating point 1 and 2 can satisfy the current power demand. However, at point 1, the instantons available torque is smaller than the torque reserve, and therefore the upshifting from point 2 to point 1 is prohibited.

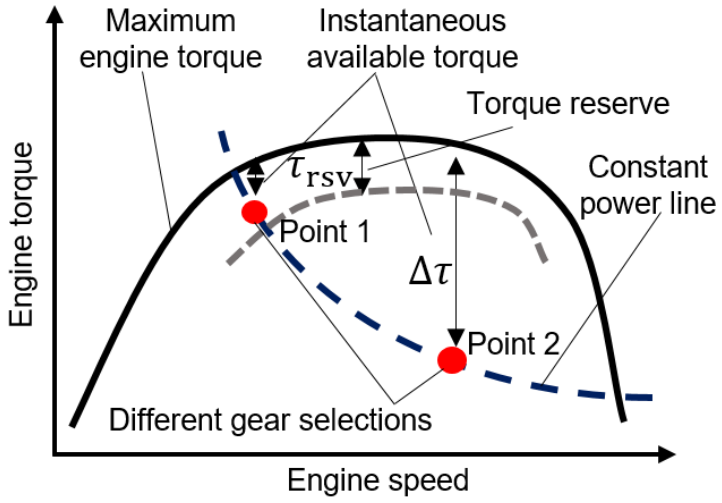

Fig.6.3 Illustration of the torque reserve

To obtain the upshift speeds in the middle torque region, the vehicle speed and torque demand are discretized into grids. For every vehicle speed and torque demand, the algorithm compares the fuel rate of the current gear and that of the next gear, assuming the same power demand can be met. The algorithm finds the gear selection that has the lower fuel consumption, while satisfies the torque reserve as described in (6.1) and (6.2):

$$\text{argmin.}\, n\, \dot{\text{m}}[w(n), \tau(n)] \quad (6.1)$$

$$\text{s.t.}\, \Delta\tau(n) > \tau_{\text{rsv}} \quad (6.2)$$

Where, $\dot{m}$ is the fuel rate function. The fuel rate function is located on the engine fuel map based on engine speed w, and engine torque τ, which both depend the gear selection n. The constraint states the instantaneously available torque $\Delta\tau$, which is a function of gear selection, needs to be greater than the torque reserve τ_{rsv}. Lastly, the shift speeds in the shift line need to be monotonically increasing, which ensures the greater torque demand always response to a higher shift speed.

Generating the shift map requires the maximum traction torque to optimize the maximum shift speed $v_{\max}$, and the torque reserve to optimize the shift line in the middle region of the shift map. These driving characteristics are obtained offline from the real-world driving data, which will be described in the next section.

6.3 Characterizing the Driving Cycle

The shift maps can be generated based on the maximum traction torque and the torque reserve, which can be obtained from the driving cycle. The process of obtaining these metrics from the driving data, as shown in Fig. 6.4, is detailed in this section.

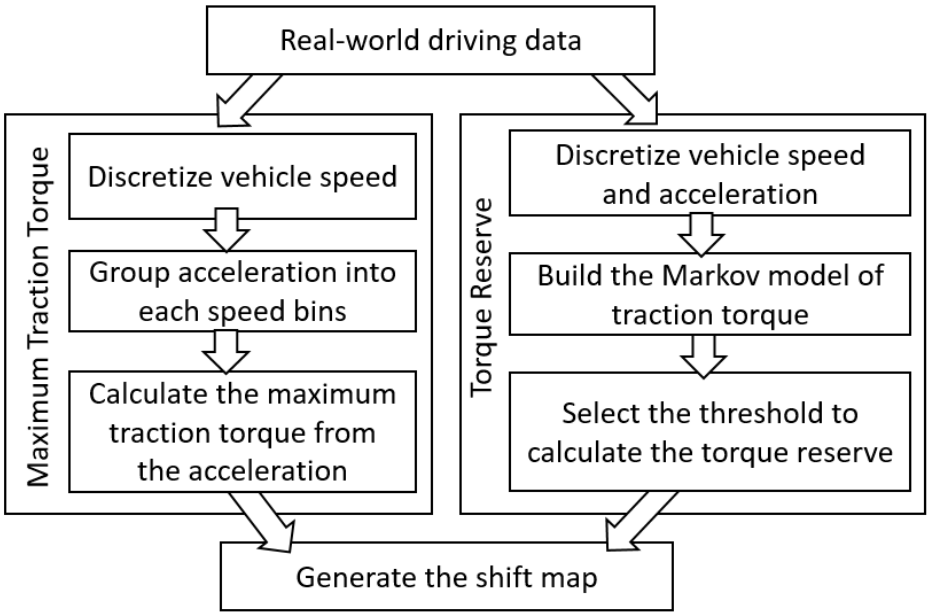

Fig.6.4 Schematic of the driving cycle characterization pipeline

Real-world driving data was collected by the industry partner to analyze the difference between the relaxed and aggressive driver. The driving data was acquired in a city driving environment with moderate traffic on a flat terrain. The different driving behavior was produced by the driver mimicking the aggressive and relaxed driving behavior. Each driver completed the cycle twice. The first time mimicking aggressive driving behavior and the second time mimicking relaxed driving behavior. The data was then processed offline to obtain the driving characteristics.

6.3.1 Maximum Traction Torque

To obtain the maximum traction torque, the vehicle speed is discretized into small intervals or bins. At each time step, the vehicle acceleration is grouped into the corresponding speed bin. The maximum traction torque at the wheels is then calculated from the vehicle speed, the maximum acceleration, and the rolling resistance and

aerodynamic drag coefficients. Since the maximum acceleration can be noisy, a threshold (98 percentile) is used to replace the maximum acceleration. Fig.6.5 shows the average maximum traction torque of the aggressive, relaxed and average drivers at different vehicle speeds. The aggressive drivers have higher maximum traction torque than the relaxed drivers, and the value is closer to the limit of the maximum traction torque the vehicle can provide at each gear.

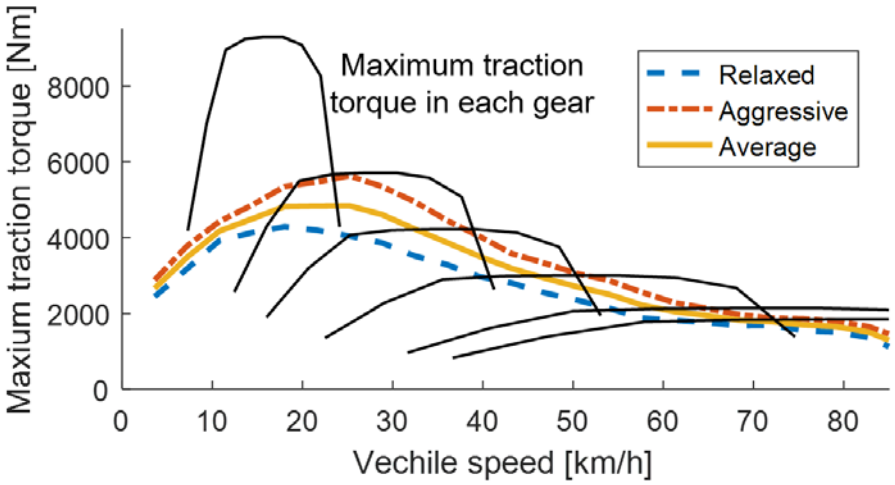

Fig.6.5 Average maximum traction torque from aggressive, average, and relaxed drivers at the various vehicle speed

6.3.2 Torque Reserve

The torque reserve is defined as a 2-d matrix based on vehicle speed and current torque demand. It specifies the additional amount of torque required at certain vehicle speed and current torque demand in order to satisfy the torque demand in the next time step. The torque reserve specifies the amount of addition torque must be available at the

current load so that the engine can satisfy the driver demand immediately without downshifting.

The Markov chain model was used to represent the probability of driver action [106]. The assumption is that the future torque demand only depends on the current vehicle speed and the current torque demand. The steps to obtain the torque reserve is as follows. Firstly, the vehicle speed and current torque demand are discretized into bins. Secondly, the algorithm finds the additional torque demand at the next time step (2 seconds) and places the value into the corresponding bins. Thirdly, the torque reserve is calculated by setting a threshold on the additional torque demand. The threshold of 90 percentile and the time step of 2 seconds indicate the amount of additional torque needs to satisfy 90 percent of the situation in the next 2 seconds without the need to downshift. The values of are determined by trial and error to provide robust results.

The result of torque reserve at a different vehicle speed and torque demand is a 2-d matrix, as shown in Fig.6.6. The torque reserve is higher at lower vehicle speed because the traction torque at wheels has higher value at low vehicle speed. Additionally, the torque reserve at lower current torque demand is higher because the vehicle at a lower speed is likely to accelerate in the next time step.

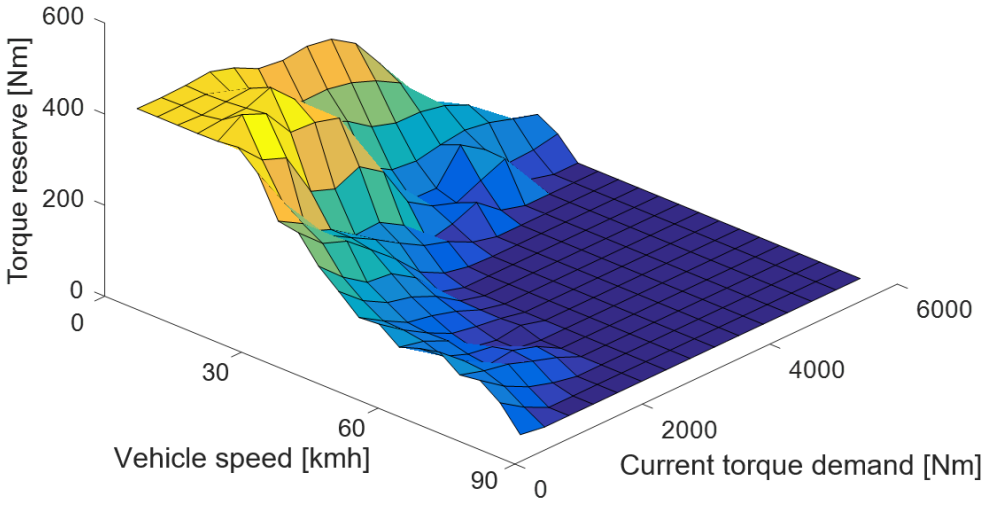

Fig.6.6 The torque reserve is 2d-matrix based on vehicle speed and current torque demand

6.4 Online Shift Map Adaptation

6.4.1 Driver Score

Although it is possible to obtain the maximum traction torque and the torque reserve online, the process would require driving the vehicle for an extended time and a large amount of memory to store the driving data. Therefore, the driver score is used to as a proxy to reconstruct the driving characteristics for the online adaption.

The driver score is based on the logistic regression classifier developed in the previous chapter. The algorithm uses features, such as the vehicle deceleration, coasting time, the kinetic energy index to evaluate the eco-driving behavior in real time.

The classifier was trained on real-world driving data of aggressive and relaxed driver. The logistic regression algorithm produces a driver score, which ranges from 0 to

1. The driver score closer to 0 represents a more aggressive driving behavior, and closer to1 representing a more relaxed driving behavior. The driver score can also be interpreted as the probability that the driver is an aggressive or relaxed driver.

6.4.2 Dimension Reduction

The maximum traction torque is a vector based on vehicle speed, and the torque reserve is a 2-d matrix based on vehicle speed and current torque demand. In order to approximate the driving characteristics using the driver score, the dimension of the characteristics needs to be reduced to a scalar. Then, a relationship between the driver score and torque reserve can be established.

The values of maximum traction torque at different vehicle speed in the real-world driving situations are highly correlated. For example, aggressive drivers have high traction torque at low speeds, they are likely to have high traction torque at high speeds as well. Based on the correlation of the values at different speeds, Principal Component Analysis (PCA) can be used to reduce the dimension of the driving characteristics. PCA reduces the dimension by preserving the large correlations [107].

The steps of the PCA are as follows. Firstly, the mean value of the maximum traction torque at different vehicle speed was calculated and subtracted from the feature vector obtained from each trip, as shown in (6.3):

$$\tilde{X} = X - \bar{X} \qquad (6.3)$$

Where X is the original maximum traction torque. $\bar{X}$ is the mean traction torque. $\tilde{X}$ is the traction torque after subtracting the mean.

Secondly, the dimension of the maximum traction torque was reduced to a scalar using the PCA, as shown in (6.4).

$$Z = V\tilde{X} \qquad (6,4)$$

Where $\tilde{X}$ is the traction torque subtracted the mean. Z is the principal components of $\tilde{X}$, and V is the eigenvectors of the covariance matrix of $\tilde{X}$. Since we want to convert $\tilde{X}$ into a scaler, only the first principal component was used.

The similar steps were conducted the torque reserve. However, the torque reserve is a 2-d matrix, which needs to be firstly vectorized by concatenating the rows together. Then the same process was conducted to reduce the dimension of the torque reserve to a scalar. After the maximum traction torque and the torque reserve are reduced to one dimension. The linear relation between these parameters and the driver score can be established.

Fig. 6.7 shows the linear functions fitted to from the driver's scores and the normalized maximum traction torque and the torque reserve. The Pearson's correlation coefficient ρ is used to quantify the correlation between the two parameters. The value of ρ ranges from -1 to 1. The closer the absolute value to 1, the stronger the correlation. The maximum traction torque and the driver score have ρ equal to -0.80. And the torque reserve and the driver score have ρ equal to -0.74. It indicates a strong correlation between these parameters and the driver score.

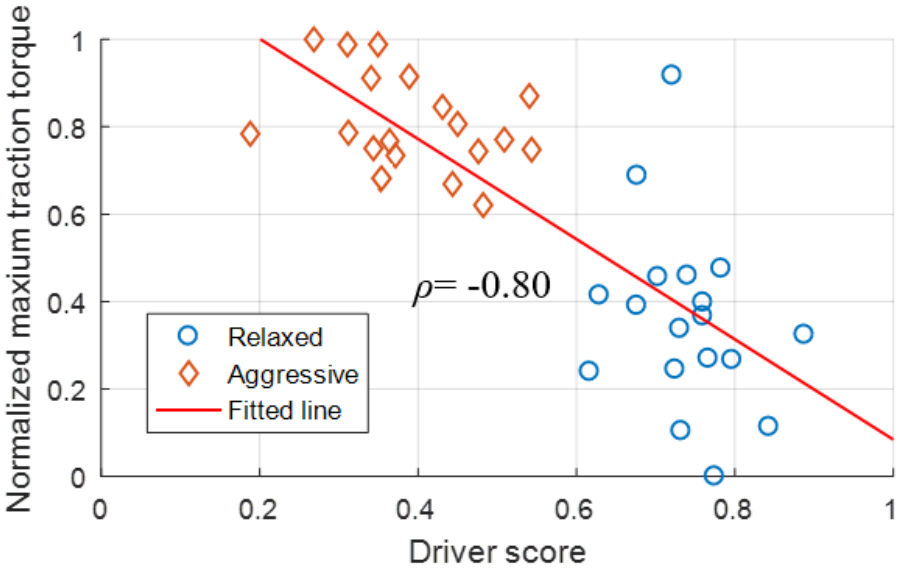

(a)

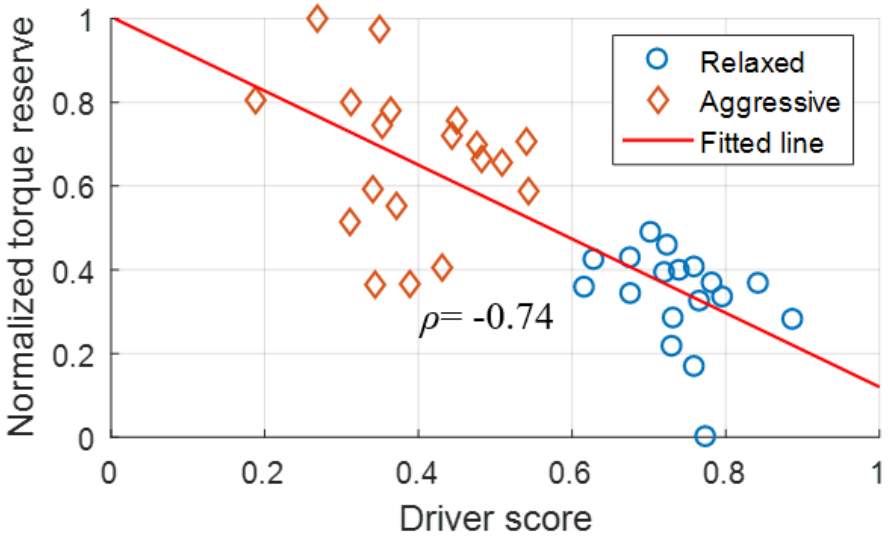

(b)

Fig.6.7 The correlation between the driver score and driving characteristics (a) The correlation between the driver score and the normalized maximum traction torque (b) The correlation between the driver score and the normalized torque reserve. A strong correlation between these parameters and the driver score can be observed

6.4.3 Approximate Cycle Characteristics

After the linear relationship between the driver score and driving characteristic are established, the driver score can be used to approximate the driving characteristic by reversing the PCA process, as shown in (6.5).

$$\hat{X} = V^T Z + \bar{X} \quad (6.5)$$

Where, $\hat{X}$ is the approximated maximum traction torque. V is eigenvectors of the covariance obtained from the PCA process. Z is the first principal component approximated from the driver score. And $\bar{X}$ is the mean value of the vectorized driving characteristic obtained in the previous steps.

By reversing the PCA process, the driving characteristics can be reconstructed from the driver score. Fig. 6.8 shows the maximum traction torque and the torque reserve reconstructed using from the driver score from 0 to 1 with 0.2 increments. In Fig. 6.8 (a), it can be observed that the more aggressive driving behavior demands have higher maximum traction torque. In Fig. 6.8 (b), the 2-d matrix of vehicle speed and current torque demand is reshaped into a vector by concatenating the rows of the matrix. It can be observed that the more aggressive driving behavior demands higher torque reserve.

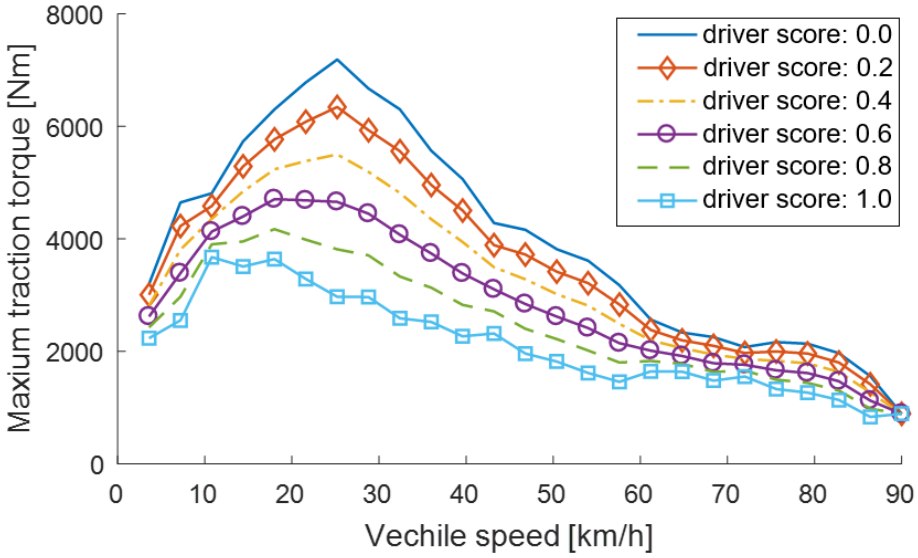

(a)

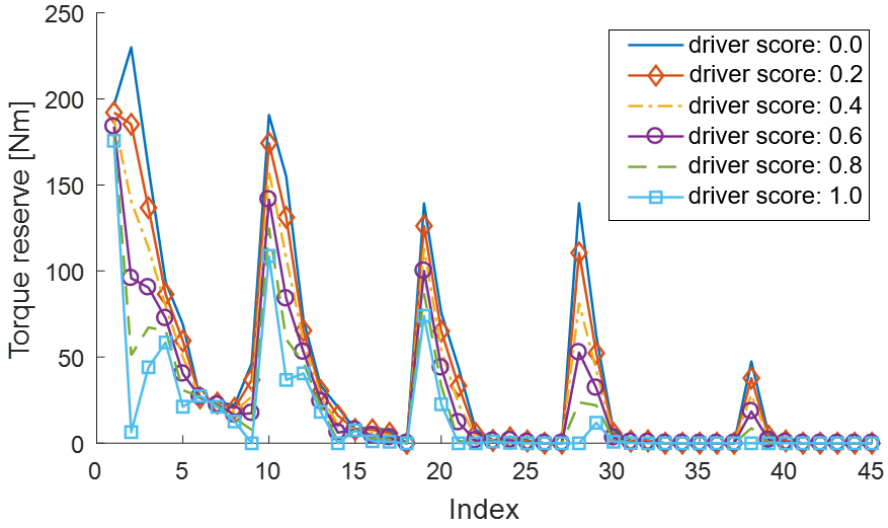

(b)

Fig.6.8 Driving characteristics reconstructed from different driver scores (a) The maximum traction torque reconstructed from different driver scores, (b) The torque reserve reconstructed from different driver scores.

In the situation that the vehicle parameters can change. The method can be revised to base on vehicle acceleration to account for different vehicle parameters. For example, if the vehicle weight changes, the new maximum traction torque can be calculated from the vehicle acceleration and the estimated vehicle mass.

6.4.4 Generate Shift Maps from Driver Scores

After the maximum traction torque and torque reserve are reconstructed from the driver score, the shift maps can be generated from these driving characteristics.

Fig. 6.9 shows the upshift and downshift maps generated for the driver score 0 to 1 with 0.2 increments. The more aggressive shift maps upshift at a higher vehicle speed at wide-open-throttle position due to the higher maximum traction torque. The aggressive shift maps also upshift at the higher throttle position than the relaxed maps at the same vehicle speed, due to the higher torque reserve.

The downshifting maps are generated that if the throttle demand is higher than 80 percent, the transmission downshifts to a lower gear to provide more traction torque. The hysteresis (4 km/h) is added to the maximum and minimum shift speed between the upshift and downshift lines. The hysteresis helps to ensure a more robust shifting due to speed fluctuation, which often occurs during shifting due to the torque interruption.

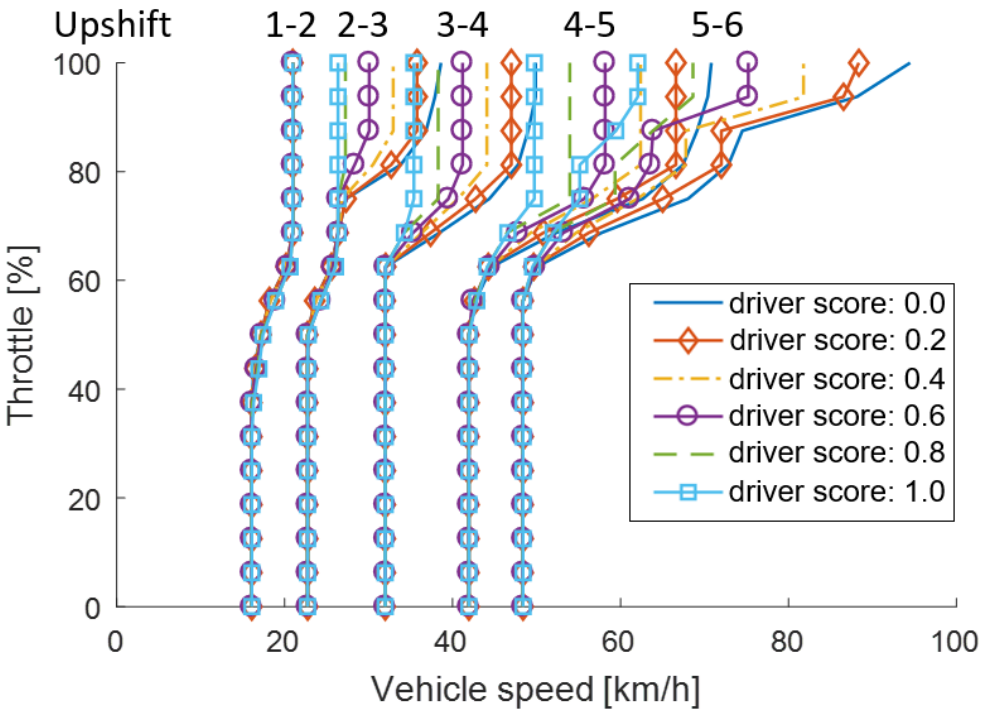
Upshift
1-2
2-3
3-4
4-5
5-6
Throttle [%]
Vehicle speed [km/h]
driver score: 0.0
driver score: 0.2
driver score: 0.4
driver score: 0.6
driver score: 0.8
driver score: 1.0

(a)

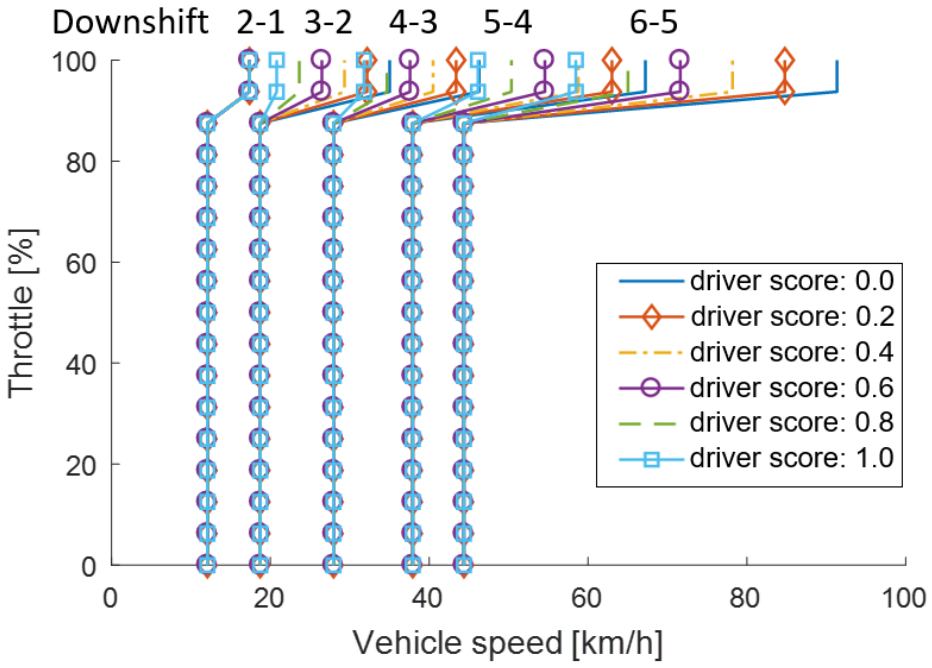
Downshift
2-1
3-2
4-3
5-4
6-5
Throttle [%]
Vehicle speed [km/h]
driver score: 0.0
driver score: 0.2
driver score: 0.4
driver score: 0.6
driver score: 0.8
driver score: 1.0

(b)

Fig.6.9 The upshifting and downshift maps (a) The upshifting map correspond to different driver scores, (b) The downshifting map correspond to different driver scores

6.5 Vehicle Model

The impact of different shift maps on the fuel consumption and drivability will be evaluated in the simulation using the real-world driving data. The vehicle simulation can be categorized into the backward-facing model and the forward-facing model [108]. The backward-facing model uses the quasi-static states of the powertrain model and does not require a driver model. However, it gives very limited information about drivability. On the other hand, the forward-facing model uses a driver model to provide propulsion torque and brake torque to satisfy the speed profile. The forward-facing model is chosen because it provides more information on drivability. The schematic of the vehicle model is shown in Fig.6.10.

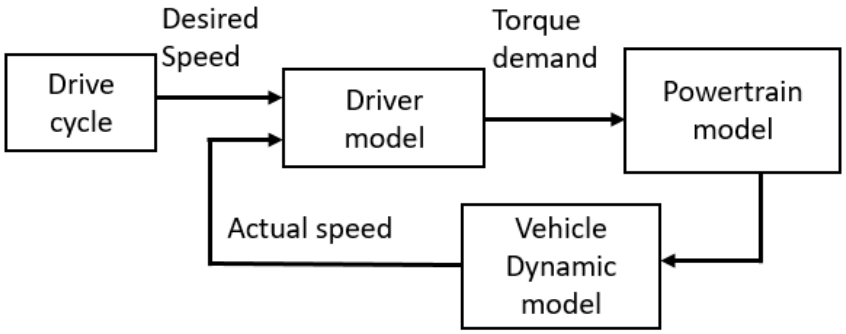

Fig.6.10 Schematic of the forward-facing vehicle simulation

The driver model consists of three components: the speed feedforward controller, the speed feedback controller, and the distance feedback controller, as shown in Fig.6.11. The speed feedforward controller previews the speed profile in the next two seconds. The

speed feedback controller uses the Proportional-Integral control to allow the vehicle to follow the desired speed trace. The distance feedback controller will compensate the difference in trip distance and ensure that the vehicle travels the same distance as the desired speed profile. The speed profile is not imposed onto the vehicle model, but a relatively small margin of error between the actual and desired vehicle speed is mandatory. The low-pass filter is used to limit high-frequency driver compensation [109].

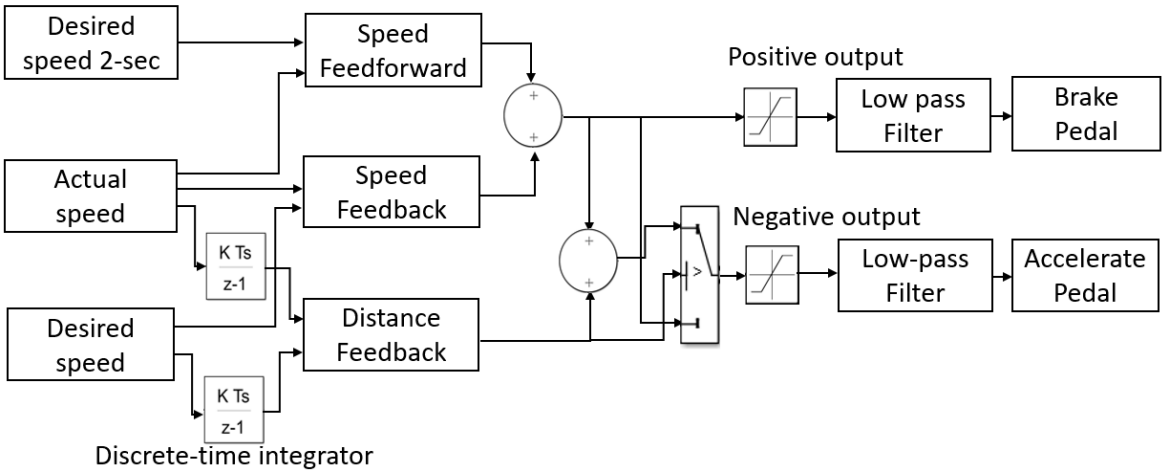

Fig.6.11 Schematic of the driver model

The vehicle used in the simulation is an 8700 kg medium duty truck, with a 6-speed automatic transmission. The vehicle has a conventional powertrain, which consists of the engine, torque converter, transmission, and the final drive. The engine model includes a transient model. The fuel delay is modeled as a lag filter [110]. The torque converter is modeled based on the k-factor. Table 1 and Fig.6.12 shows the parameters and the picture of the vehicle used for the data collection.

Table 6.1. The parameters of vehicle used for the data collection

Table 6.1. The parameters of vehicle used for the data collection

Vehicle weight	8700 kg
Maximum engine torque	595 Nm at 1800 rpm
Transmission gear ratio	3.094, 1.809, 1.406, 1,0.711, 0.614
Torque converter maximum torque ratio	1.79

Fig 6.12 Picture of the vehicle used for the data collection

6.6 Drivability Metric

Drivability is a very subjective metric, which often refers to driver's impression of the overall driving quality, such as pedal responsiveness, operating smoothness and driving comfort [85].

Metrics to objectively evaluate the drivability have been discussed in the previous literature. The study by Wei and Rizzoni [85] has quantified the pedal hesitation, delay, and sluggishness using metrics such as the root mean square (RMS) value of the vehicle

acceleration and jerk. A neural network's system has been developed using a variety of relevant conscious or subconscious criteria to provide the assessment of the overall drivability [9]. The study by List and Schoegg [10] has detected the driving behavior and adapted the vehicle character online to increase the vehicle sportiness and spontaneity.

Among all the drivability metrics, vehicle's accelerating response is the most relevant to the transmission shift strategy. The accelerating response is closely related to the torque reserve [11], which is defined as the amount of the torque the engine can provide instantaneously without downshifting.

A new drivability metric is defined as the Speed Root Mean Square (SRMS) error between the desired and actual vehicle speed, as in equation (6.6):

$$\text{SRMS} = \sqrt{\frac{1}{n}\sum_{i=1}^{n} [\max(v_{di} - v_{ai}, 0)]^2} \text{ , (when } a_i > a_t) \qquad (6.6)$$

Where v_{di} and v_{ai} are the desired and actual vehicle speed at the time step i. The maximum function ensures v_{di} is greater than v_{ai}, otherwise it the value 0 will be used. The metric measures the vehicle's capability to follow the speed profile during the acceleration events, which is indicated by a_i, the acceleration at time step i is greater than a threshold a_t.

The new drivability metric describes the vehicle's ability to follow the desired speed trace during the acceleration events in the simulation. For example, if a relaxed shift map is applied to an aggressive driving cycle, the vehicle will have difficulties following the desire speed trace.

As illustrated in the Fig.6.13, two simulations were conducted, with the aggressive shift map and the relaxed shift map. The one using the aggressive map can follow the desired speed profile closely. However, the one using the relaxed map has a large difference to the desired speed during the accelerating events.

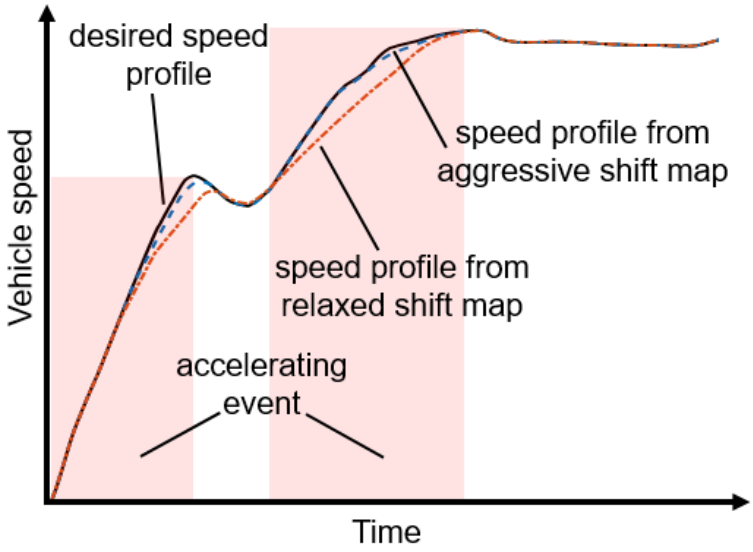

Fig. 6.13 Illustration of the impact of shift map on drivability. The speed trace of relaxed shift map has difficulties to follow the desire speed profile.

6.7 Simulation Results

In this section, the shift maps are tested in a vehicle simulation to evaluate the impact on drivability and the fuel consumption.

Firstly, the acceleration test was conducted to evaluate the wide-open-throttle performance. Secondly, a shift map adaptation strategy was evaluated using the real-world driving. Thirdly, the trade-offs between the fuel consumption and the drivability

were assessed based on the driving cycles of different driver aggressiveness. And lastly, an energy audit was conducted to analyze the contribution of different aspects to the fuel consumption reduction.

6.7.1 Acceleration Test

The acceleration test is conducted to evaluate the vehicle's performance at the wide-open-throttle position. The 0-100 km/h acceleration time is used as the performance metrics. Six shift maps were generated based on the driver score ranges from 0 (most aggressive) to 1 (most relaxed) in 0.2 increments. The speed profile and the 0-100 km/h acceleration time results of each shift map are shown in Fig.6.14.

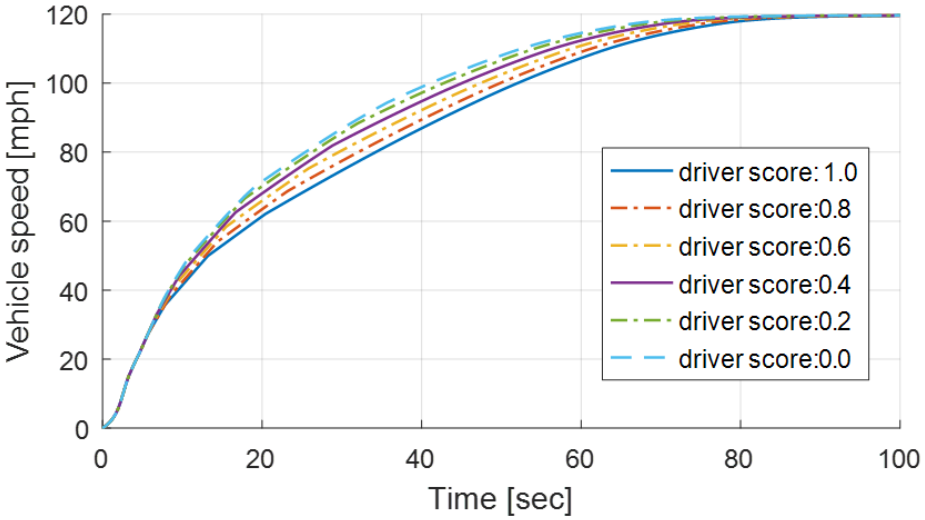

(a)

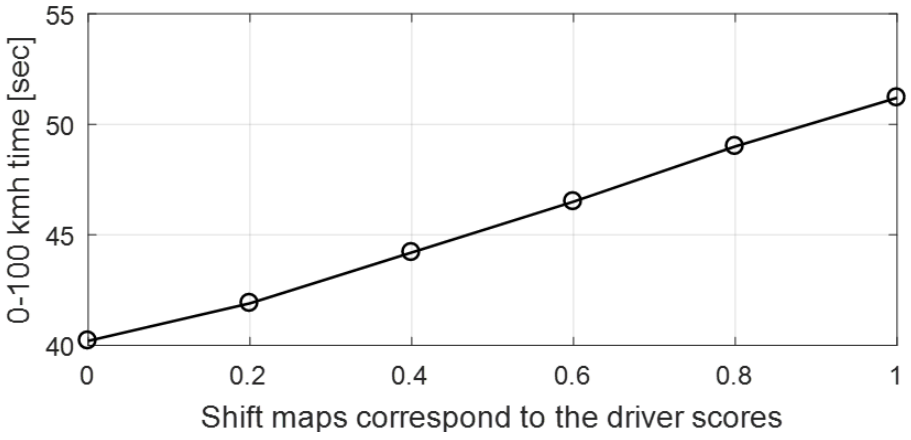

(b)

Fig. 6.14. Acceleration test results (a) The vehicle speed trace using different shift maps, (b) The 0-100 km/h time result of different shift maps,

There is a 21.5 percent difference in the acceleration time between the most aggressive shift map (40.2 second) and the most relaxed shift map (51.2 seconds). The relaxed maps have longer acceleration time than the aggressive maps because they upshift at lower engine speed which reduces the maximum traction torque. On the other hand, the more aggressive shift maps upshift at the engine speed closer to the intersection of the maximum torque curve of each gear, which will result in higher acceleration performance.

6.7.2 Adaptation Strategy

The 0-100km/h time measures the maximum acceleration performance of the shift maps. However, the driver aggressiveness also affects the perceived drivability. For example, If the driver has a relaxed driving behavior, it is possible to satisfy the driving

demand using a relaxed shift map. In this section, the adaptation strategy is demonstrated using the real-world driving data of different aggressiveness.

The adaptation strategy is described as follows. The fleet owner can select the most aggressive driver score that is allowed. If the driver exceeds the threshold, the shift strategy will cease to attempt to accommodate the drivability and impose a less aggressive shift map in order to reduce the fuel consumption.

Three trips from the data set were selected with the driver score of low (0.19), middle (0.51), high (0.89) to represent relaxed, normal, and aggressive driving behaviors. The speed profile of the trips is shown in Fig.6.15. The three trips use the same route, however, with the different real-world driving condition such as the different traffic light patterns. The aggressive driving cycle has higher acceleration and deceleration rate. The simulation was conducted on all the three driving cycles to represent different driving cycles behaviors.

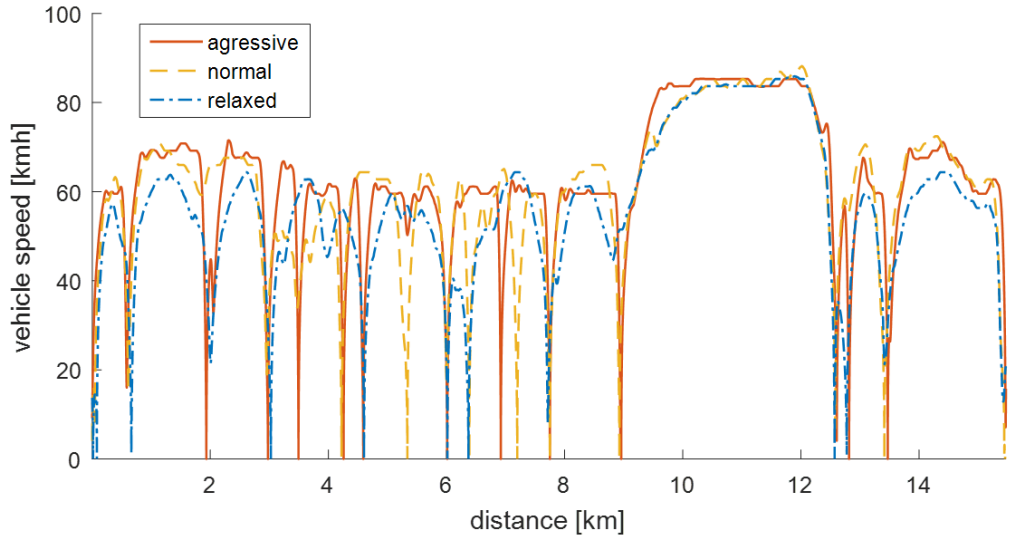

Fig. 6.15. Speed profile of the aggressive, normal and relaxed real-world driving cycle

The effect of shift strategy was evaluated in the simulation. Liter/100 km was used as the fuel consumption metric. SRMS was used as the drivability metric.

Four scenarios were tested in the simulation to demonstrate the effect of the adaptive strategy. In the first scenario, the static shift map was used during the entire driving cycle. The shift map was generated based on the average driver behavior (driver score of 0.5).

The second scenario uses the adaptive shift strategy towards drivability. The threshold of the most aggressive driver score is 0.2. The shift strategy will accommodate towards drivability until the driver score drops below 0.2.

The third scenario uses the adaptive shift strategy biased towards fuel consumption

. The threshold of the most aggressive driver score is 0.8. If the driver score falls below 0.8, the shift strategy will impose a relaxed shift map (based on driver score 0.8) to reduce the fuel consumption.

In the last scenario, Dynamic Programming (DP) was used to obtain the optimal shift schedule, which serves as the benchmark. The Dynamic Programming was implemented base on the assumption that the future speed profile of the driving cycle is known.

The steps of the Dynamic Programming is described as follows. Firstly, the states are defined as the gear selection at each location. The cost function is based on fuel rate and the transition cost for gear shifting to prevent the gear hunting. Secondly, the traction torque at the wheels is calculated from the vehicle speed profile. Then, the engine speed

and engine torque to satisfy the traction torque at wheels at each gear are calculated. Thirdly, the fuel rate at each gear is looked up from the fuel map based on the engine speed and engine torque. And lastly, the cost function was solved from the destination to the origin to find the gear selection that satisfies the torque demand with the lowest fuel rate.

A section of the speed profile response to the different shift strategies is shown in Fig.6.16. It can be observed that during the sharp acceleration event, the relaxed shift schedule has difficulty in following the target speed trace. This is because the relaxed map tends to shift at low engine speed, which reduces the vehicle maximum acceleration capacity. The relaxed speed profile also reduces the deceleration during braking to compensate for the loss of distance travel during the acceleration.

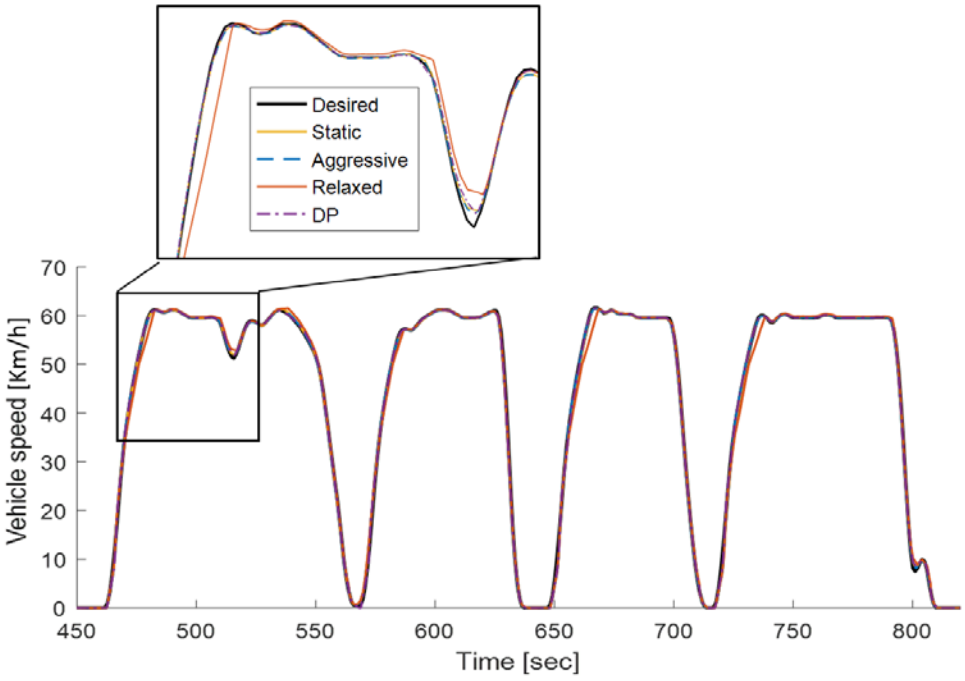

Fig.6.16 The speed profiles response different shift schedule.

The fuel consumption and drivability results in each driving cycle are shown in Table 6.2 and 6.3.

Table 6.2. Fuel consumption L/100 km results

	Aggressive cycle	Normal cycle	Relaxed cycle
Static map	20.94	15.95	14.79
Adaptive map biased towards fuel consumption	20.61 (-1.6%)	15.82 (-0.8%)	14.77 (-0.1%)
Adaptive map biased towards drivability	21.12 (+0.9%)	15.97 (+0.1%)	14.80 (+0.1%)
DP Solution	21.03 (+0.4%)	15.96 (+0.1%)	14.79 (+0.0%)

Table 6.3. The drivability SRMS results

	Aggressive cycle	Normal cycle	Relaxed cycle
Static Map	0.198	0.147	0.127
Adaptive map biased towards fuel consumption	0.439 (+121.7%)	0.147 (+0.0%)	0.127 (+0.0%)
Adaptive map biased towards drivability	0.185 (-6.6%)	0.140 (-4.8%)	0.126 (-0.8%)
DP Solution	0.175 (-11.6%)	0.134 (-8.8%)	0.086 (-32.3%)

The adaptive shift strategy biased toward fuel consumption has shown a 1.6 percent reduction in fuel consumption in the aggressive cycle compared with the static

map. The adaptive shift strategy biased toward drivability achieved better drivability but more fuel consumption. The Dynamic Programming result is close to the adaptive map toward drivability, because it tries to satisfy the driver demand.

6.7.3 Trade-off between Fuel Consumption and Drivability

Fuel consumption and drivability are often competing metrics. In this section, the trade-off between the two metrics is evaluated in the simulation using the real-world driving cycles of different driver aggressiveness.

Six shift maps, generated from the driver score from 0 to 1 with 0.2 increments, were tested on the aggressive, normal, and relaxed driving cycles. The result of drivability and fuel consumption in each cycle is shown in Fig.6.17.

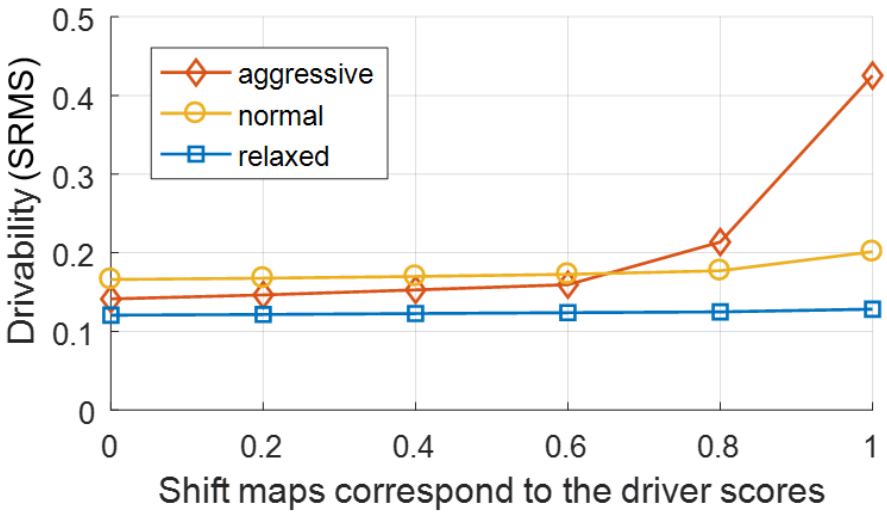

(a)

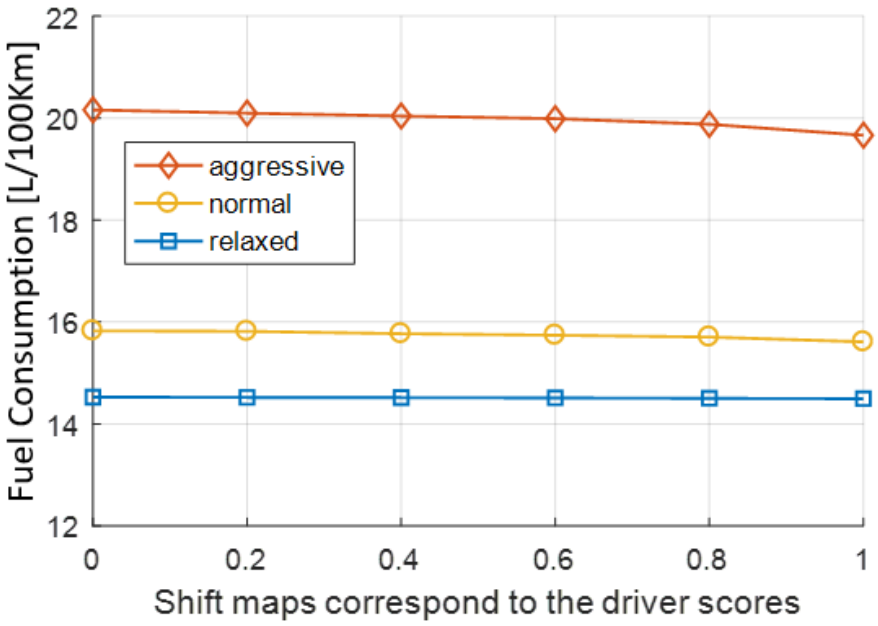

(b)

Fig 6.17. Drivability and fuel consumption results (a) The drivability results from different shift maps on the aggressive, normal and relaxed cycle. (b) The fuel consumption results from different shift maps on the aggressive, normal and relaxed cycle.

In Fig.6.17. (a), the SRMS between the desired and actual speed trace increases as the shift map became more relaxed, which indicates the loss of drivability. In the situation of using the relaxed maps (generated from driver score 0.8 and 1) for the aggressive driving cycle, the SRMS increases largely. This is because the relaxed shift maps have the lower acceleration capacity and therefore resulting in the large error between the desired and actual speed profile. On the other hand, the vehicle fuel consumption decreases as the shift map become more relaxed for all the three driving cycles, as shown in Fig.6.17 (b). Moreover, the higher percentage gain can be achieved

for the aggressive cycle (2.46 percent) compared to that of the relaxed cycle (0.21 percent).

The trade-offs between the fuel consumption and drivability are shown in Fig.6.18. The values are normalized as percentage increase based on the results of the most aggressive shift maps.

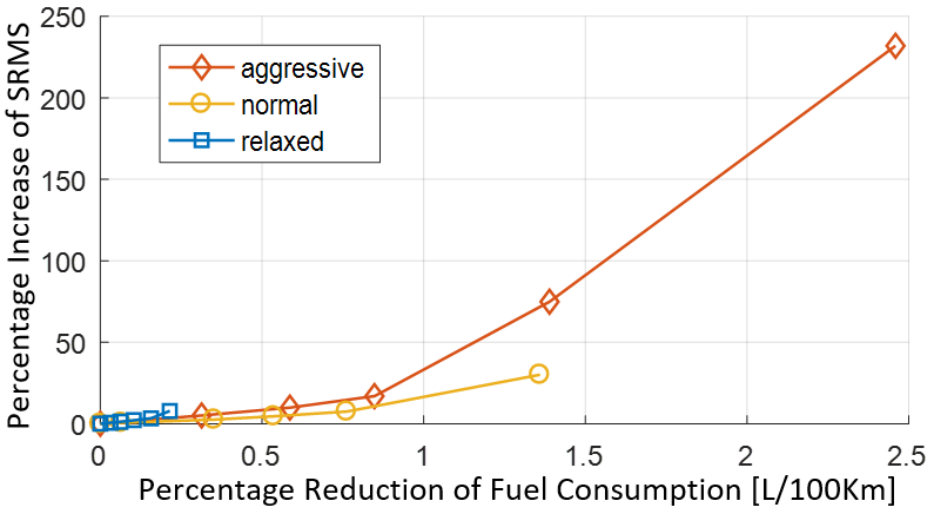

Fig.6.18. The trade-off between fuel consumption and drivability.

The effect of the shift maps is the most prominent in the aggressive driving behavior. A 2.46 percent reduction in fuel consumption can be achieved by changing from the most aggressive to the most relaxed shift maps. However, the drivability deteriorates significantly as indicated by the SRMS increased by 232 percent. The effect of shift maps in the normal and the relaxed driving cycle is smaller. The fuel consumption difference between the most aggressive and the most relaxed shift maps is 1.42 percent in the normal driving cycle and 0.21 percent in the relaxed driving cycle. The drivability difference on the normal and relaxed cycle is also close, about 32 percent in the normal driving cycle and 7 percent in the relaxed cycle. This is because in the less

aggressive driving cycle even the relaxed shift map can satisfy most of the driver demand.

6.7.4 Energy Audit

The energy audit was conducted in this section to analyze the contribution of the different aspects of the fuel consumption reduction between the most relaxed and the most aggressive shift maps.

The total energy consumption consists of the kinetic energy loss due to braking, energy consumed by rolling resistance and aerodynamic drag, the engine energy loss, and energy loss during idling, as shown in (6.7):

$$E_f = (E_k + E_r)/\eta + E_i \quad (6.7)$$

Where E_f is the energy in the fuel, E_k is kinetic energy loss during braking, E_r is the energy consumed by rolling resistance and aerodynamic drag, η is the average engine efficiency, and E_i is the energy loss during idling.

The energy consumed by rolling resistance and aerodynamic drag is calculated as the sum of the rolling resistance and aerodynamic drag multiplied by the distance of the road section as shown in (6.8):

$$E_r = E_{ad} + E_{rr} = \sum(mgC_r + C_{dL}v_i^2)\Delta d_i \quad (6.8)$$

Where C_r is the rolling resistance coefficient, C_{dL} is the lumped aerodynamic drag coefficient and Δd is the small distance traveled in time step i.

The kinetic energy consumed during braking is calculated from the speed profile when vehicle speed at the next time step is smaller than the current vehicle speed. The

energy consumed by rolling resistance and aerodynamic drag is subtracted as shown in (6.9).

$$E_k = \sum \left[\frac{1}{2} m(v_{i+1}^2 - v_i^2) - (mgC_r + C_{dL} v_i^2)\Delta d_i\right] \text{ when } v_{i+1} < v_i \qquad (6.9)$$

Since the same driving cycle is used, the energy consumed during idling is the same. The difference mainly comes from, kinetic energy E_k, resistance energy E_r, and average engine efficiency η. The kinetic energy and resistance energy from the most aggressive and the most relaxed shift strategy were placed into equation (6.7) one parameter at a time, to calculate the contribution of each individual parameter to the change of total fuel consumption.

The result of the contribution of kinetic energy, resistance energy, and engine efficiency are shown in Fig.6.19.

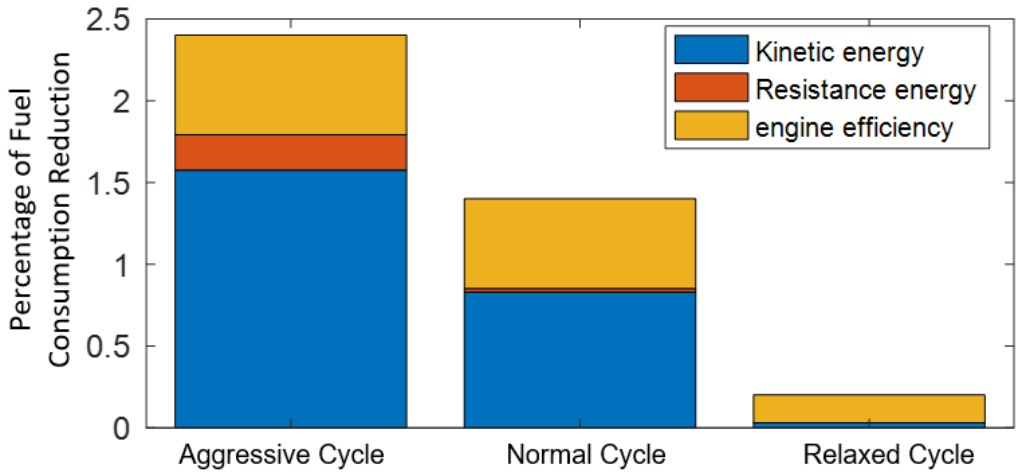

Fig.6.19. The contribution of different aspects to the fuel consumption reduction

In the aggressive cycle, the majority of fuel consumption reduction is obtained from reducing the kinetic energy (1.6 percent). In the normal driving cycle, the reduction of the kinetic energy and increasing engine efficiency contribute to 0.82 percent and 0.52

percent of the fuel consumption reduction, respectively. In the relaxed cycle, the majority of the gain is come from engine efficiency (0.17), because both the aggressive and relaxed map can satisfy the desired speed profile.

6.8 Conclusion

In conclusion, a new adaptive shift strategy have been demonstrated, which can adjust the shift points to different vehicle parameters and driver behavior. The process is illustrated in Fig.6.20. The driving data is passed to the WRLS algorithm to estimate the vehicle rolling resistance and aerodynamic drag coefficient. Subsequently, the vehicle parameters are used to predict the vehicle road load. The driver scoring algorithm evaluates the driving behavior in real time. Based on the limits imposed by the fleet owner, driver score is used as a proxy to match the torque reserve. Finally, the transmission shift controller uses the information of and road load and torque reserve to optimize the shift map.

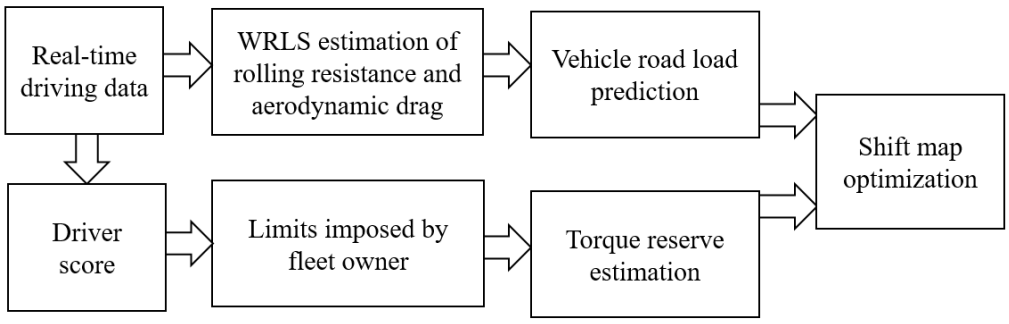

Fig.6.20. The flow diagram of the adaptive shift strategy using the information from the vehicle parameters estimator and the driver scoring algorithm

An objective drivability metric is defined to describe the vehicle's ability to follow the desired speed trace during the acceleration. The adaptive shift strategy was tested with real-world driving data in a vehicle simulation and can achieve 0.21 to 2.46 percent fuel consumption reduction depended on the driver aggressiveness. The adaptive shift strategy can reduce the initial calibration effort and allow the fleet owners to decide the trade-offs between fuel consumption and drivability for different vocations.

CHAPTER SEVEN

CONCLUSIONS AND FUTURE WORK

7.1 Conclusion

Proper transmission shift strategy is crucial for the vehicle fuel consumption and drivability. The wide variety of vehicle configuration and the different fuel consciousness pose a challenge for the shift strategy of the commercial vehicle. Adaptive shift strategy can potentially reduce the initial calibration efforts by adjusting the shift map based on the road load and driver behavior on-the-fly. However, it requires the information about vehicle road load and the driving behavior as a prerequisite.

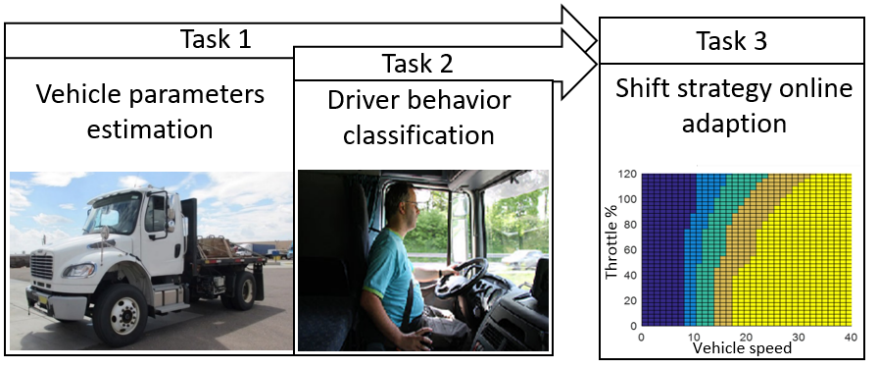

Fig.7.1 The tasks comprising this dissertation.

This dissertation has considered three questions raised by the overarching goal to develop an adaptive shift strategy algorithm, as shown in Fig.7.1. The first question is to estimate the vehicle road load. To calculate the road load, the vehicle rolling resistance and aerodynamic drag coefficient need to be estimated, which have not been sufficiently addressed in published literature. A new algorithm is proposed for using the vehicle

longitudinal dynamic during the constant-speed event and save the measurement at each speed segments to overcome the problem of lack of persistence excitation during the constant-speed event. The algorithm was demonstrated in the simulation environment using the real-world driving data and achieved 5 percent accuracy in the aerodynamic drag coefficient. However, the estimation of rolling resistance coefficient is less accurate due to the higher sensitivity to the input noise.

The second question is the need to evaluate the driving behavior. We aim towards finding a robust method across different driving cycles and vehicle types. A driver behavior scoring algorithm was proposed based on the supervised learning approach. Twenty-six hours of real-world driving data were collected by driver mimicking aggressive and relaxed driving behavior. The time-series driving data are converted to symbolic data to facilitate feature extraction. The features are extracted based on microtrips, which are segmented by their average speed to reduce the influence of different driving cycles. The logistic regression algorithm is chosen because the classification rule is explicit, and computation and memory efficient. The classification accuracy was used as the performance metric, and the algorithm achieved on average 82.7 percent classification accuracy. The robustness of the algorithm has been demonstrated on a wide variety of vehicle and driving cycles. Lastly, a strong correlation between driver score and the real-world fuel consumption have been found, which shows the driver score as a good indicator for driver aggressiveness.

The third question is to synthesize the information of vehicle parameters and driver score into the adaptive shift strategy. A new adaptive shift strategy was proposed,

which is optimized based on the maximum traction torque and torque reserve. Torque reserve effectively represents the drivability objective. Obtaining these parameters online requires the vehicle to be driven for an extended time, and therefore driver score was used to approximate these parameters. The adaptive shift strategy provides the fleet owner a way to choose between fuel consumption and drivability. If the driver aggressiveness exceeds the limit, a relaxed shift map will be imposed to reduce fuel consumption. The adaptive shift strategy was compared with the static shift map in the vehicle simulation using the real-world driving data and have shown potentially 0.21 to 2.46 percent fuel consumption reduction depended on the driving cycle.

The algorithms proposed in this dissertation are computationally and memory efficient. Therefore, they are suitable to be implemented in the transmission control unit to reduce the initial calibration effort for different vehicle configurations and allows the fleet owner to decide the trade-offs between fuel consumption and drivability based on their fuel consciousness.

7.2 Future Work

In this dissertation, the shift map was optimized by the characteristics of the driving cycle, which were approximated by driver score. However, the exact further driving information is considered as unknown. The recent trend in advanced powertrain control strategies is to connect the vehicle to the cellular network or the Internet to obtain the future driving information [111].

Base on the uncertainty of the future driving information, the situations can be classified into three categories. Firstly, both knowledge of upcoming terrain and traffic conditions are available. The study by Hellström et al. [76] proposed a look-ahead control algorithm based on Dynamic Programming for a conventional heavy diesel truck to achieve optimal velocity profile and gear selection. The study by Chen et al.[112] and Zhang and Vahidi [113] has shown the benefit of using the preview of terrain information in the Energy-management strategy (ECMS) of the plug-in hybrid electric vehicle. Secondly, the terrain is known, but the speed profile needs to be estimated. It is a more realistic assumption because in the real-world driving when the route is chosen the grade can be known exactly through vehicle navigation system, but the speed profile cannot be known in advance. The velocity can be estimated using real-time traffic data streams or by using historical traffic data[114][115][116]. Lastly, only the statistic of the route is known. The geographic region that the vehicle is driven is known, and the vehicle route is assumed to be unknown in advance. The study by Kolmanovsky and Filev [117], McDonough et al.[118] [119] proposed a method to customized vehicle speed control by applying off-line stochastic dynamic programming to construct an optimal control policy or best on-average performance. The terrain and traffic patterns are modeled stochastically as two Markov Chains. Furthermore, the Markov transition model can be learned onboard as proposed in the study by Hoekstra et al. [106].

Another aspect is on how to how to induce the eco-driving behavior to reduce the real-world fuel consumption. In this dissertation, we tried to change the shift schedule to reduce the fuel consumption of aggressive driver, which has shown can achieve

potentially 2.46 percent of improvement. Further improvement can be achieved if throttle control can be use to modify the speed profile. In the study by Mensing et al.[44], the speed profile is formulated as minimizing the fuel use and is solved by Dynamic Programming. In the real driving situations, the future driving situation has more uncertainty, so it is often model as Markov chain model. Model Predictive Control (MPC) has been proposed to achieve more fuel efficient driving using the stochastic property of the future driving. The study by Kamal et al.[120][47] and Chen et al.[121] derive the control inputs based on the driving conditions and the fuel consumption index which represent eco-driving. In the case of car following, the study by Zhang and Vahidi [45] and Mcdonough et al.[122] estimated the probability distribution of the front vehicle position as the constraint to the MPC problem. In summary, with the future driving information and the throttle control to induce the eco-driving, the vehicle fuel consumption can be further reduced.

APPENDICES

Appendix A

Algorithms

Alg.4.1 Measurement Update

Input: extract_data – whether the data extraction criteria are satisfied, v –vehicle speed, t_e– engine torque, ω_e – engine speed, α – road grade, a – longitudinal acceleration, Y– average road load, N– number of measurements

1. **if** extract_data ==Ture
2. $y \leftarrow$ Compute_Road_Load (v, t_e, ω_e, α, a)
3. $i \leftarrow$ Find_Speed_Segment (v)
4. $y_i \leftarrow$ Adjust_Load (v, i, y)
5. $Y, N \leftarrow$Calculate_Recursive_Average (Y, N, y_i, n_i)
6. **end if**

Output: Y– average road load, N– number of measurements

Alg. 4.2 Weighted Recursive Least Square (WRLS)

Input: conduct_estimation – whether to conduct the state estimation, Y– average road load, N– number of measurements

1. **if** conduct_estimation == Ture
2. **for** i =1:length(Y)
3. **if** $n_i > 0$
4. $R_i \leftarrow$ Compute_Weight (n_i)
5. $\hat{\theta} \leftarrow$ RLS ($\bar{y}_i, R_i$)

6. **end if**

7. **end for**

8. **end if**

Output: $\hat{\theta}$ –state estimation

Alg.5.1 Convert time-series data in events

Input: (v, a_c, t_p) current driving data (v –vehicle speed, a_c–acceleration, t_p–throttle position)

1. $p_1 \leftarrow$ assign a primitive to the current driving data

   (v, a_c, t_p)

2.**if** p_1 the current primitive $\neq p$ the previous primitive

3. update the end speed: $v_1 \leftarrow v$

4. save (p_0, v_0, v_1, t) as a driving event

5. initialize a new driving event: $p \leftarrow p_1$, $v_0 \leftarrow v$,

   $v_0 \leftarrow v$, $t \leftarrow 0$

5. **else**

6. increment the event duration $t \leftarrow t + \Delta t$

7.**end if**

Output: (p, v_0, v_1, t) - driving event (p-primitive, v_0–start speed, v_1–end speed, t–duration)

Alg. 5.2. Driver scoring algorithm

Input: (p, v_0, v_1, t)–driving event, x–feature vector, *microtrip_start*–whether a micortirp have started

1. **if** a microtrip has started: *microtrip_start* == True
2. **if** the previous microtrip ends (an idling event occur and the duration exceed a limit): p= i and $t > t_m$
3. end the microtrip: *microtrip_start* ← False
4. x ← update feature vector from the driving event (p, v_0, v_1, t)
5. s ← calculate the microtrip score (x)
6. S ← calculate the driver score using moving average (s)
7. **else if** a new microtrip starts (a accelerating event occurs at low speed): p =a and $v_0 < v_m$
8. s ← calculate the microtrip score (x)
9. S ← calculate the driver score using moving average (s)
10. x ← initialize the feacture vector
11. x ← update feature vector from the driving event (p, v_0, v_1, t)
12. **end if**
13. **end if**
14. **else**
15. **if** a new microtrip starts: $p = a$ and $v_0 < v_m$

16 *microtrip_start* ← True

17 **end if**

18. **end if**

Output: *S*–driver score, *x*–feature vector, *microtrip_start*– whether a micortirp have started

REFERENCES

[1] M. Margreta, C. Ford, and G. Ryan, “U.S. Freight on the Move: Highlights From the 2012 Commodity Flow Survey Preliminary Data,” 2014.

[2] “Oak Ridge Laboratory National Transportation data book, Edition 35,” 2016. [Online]. Available: http://cta.ornl.gov/data/index.shtml.

[3] Federal legislation, “Greenhouse Gas Emissions Standards and Fuel Efficiency Standards for Medium- and Heavy-Duty Engines and Vehicles; Final Rule,” *Fed. Regist.*, vol. 76, no. 179, 2011.

[4] 21st Century Truck Partnership, “Roadmap and Technical White Papers,” 2013.

[5] U. D. of Transportation, “Impact of Transmission Technologies on Fuel Efficiency – Final Report,” no. August, 2012.

[6] S. Bai, J. Maguire, and H. Peng, *Dynamic Analysis and Control System Design of Automatic Transmissions*. SAE International, 2013.

[7] *Design Practices Passenger Car Automatic Transmissions*, 4th ed. SAE International, 2012.

[8] J. B. Heywood, “Internal Combustion Engine Fundamentals,” pp. 217-218-840-862-875, 1988.

[9] H. O. List and P. Schoeggl, “Objective Evaluation of Vehicle Driveability,” *Sae*, no. 724, 1998.

[10] P. Schoeggl and W. Kriegler and E. Bogner, “On-board optimization of driveability character depending on driver style by using a new closed loop approach,” no. 724, 2001.

[11] N. D. Viet, “Gear Shift Strategies for Automotive Transmissions,” Eindhoven Univeristy, 2012.

[12] K. Newman, J. Kargul, and D. Barba, “Development and Testing of an Automatic Transmission Shift Schedule Algorithm for Vehicle Simulation,” *SAE Int. J. Engines*, vol. 8, no. 3, pp. 2015-01–1142, 2015.

[13] M. Sivak and B. Schoettle, “Eco-driving: Strategic, tactical, and operational decisions of the driver that influence vehicle fuel economy,” *Transp. Policy*, vol. 22, pp. 96–99, 2012.

[14] H. Ohnishi, J. Ishii, M. Kayano, and H. Katayama, “Study on road slope estimation for automatic transmission control,” *JSAE Rev.*, vol. 21, no. 2, pp. 235–240, 2000.

[15] D. Swaroop, J. Karl Hedrick, and S. B. Choi, “Direct adaptive longitudinal control of vehicle platoons,” *IEEE Trans. Veh. Technol.*, vol. 50, no. 1, pp. 150–161, 2001.

[16] E. Hellström, M. Ivarsson, J. Aslund, and L. Nielsen, “Look-ahead control for heavy trucks to minimize trip time and fuel consumption,” *IFAC Proc. Vol.*, vol. 5, no. PART 1, pp. 439–446, 2007.

[17] H. K. Fathy, D. K. D. Kang, and J. L. Stein, “Online vehicle mass estimation using recursive least squares and supervisory data extraction,” *2008 Am. Control Conf.*, pp. 1842–1848, 2008.

[18] H. S. Bae, J. Ryu, and J. C. Gerdes, “Road grade and vehicle parameter estimation for longitudinal control using GPS,” *IEEE Conf. Intell. Transp. Syst. Proceedings,*

pp. 166–171, 2001.

[19] S. Mangan and J. Wang, “Development of a novel sensorless longitudinal road gradient estimation method based on vehicle CAN bus data,” *IEEE/ASME Trans. Mechatronics*, vol. 12, no. 3, pp. 375–386, 2007.

[20] P. Sahlholm and K. H. Johansson, “Segmented road grade estimation for fuel efficient heavy duty vehicles,” *Proc. IEEE Conf. Decis. Control*, pp. 1045–1050, 2010.

[21] J. Parviainen, J. Hautamäki, J. Collin, and J. Takala, “Barometer-Aided Road Grade Estimation,” *Proc. 13th IAIN world Congr.*, 2009.

[22] S. Mangan, J. Wang, and Q. H. Wu, “Measurement of the road gradient using an inclinometer mounted on a moving vehicle,” *Proceedings. IEEE Int. Symp. Comput. Aided Control Syst. Des.*, pp. 80–85, 2002.

[23] A. Vahidi, M. Druzhinina, A. Stefanopoulou, and H. Peng, “Simultaneous mass and time-varying grade estimation for heavy-duty vehicles,” *Proc. 2003 Am. Control Conf. 2003.*, vol. 6, pp. 4951–4956, 2003.

[24] M. L. McIntyre, T. J. Ghotikar, A. Vahidi, X. Song, and D. M. Dawson, “A two-stage Lyapunov-based estimator for estimation of vehicle mass and road grade,” *IEEE Trans. Veh. Technol.*, vol. 58, no. 7, pp. 3177–3185, 2009.

[25] M. N. Mahyuddin, J. Na, G. Herrmann, X. Ren, and P. Barber, “Adaptive observer-based parameter estimation with application to road gradient and vehicle mass estimation,” *IEEE Trans. Ind. Electron.*, vol. 61, no. 6, pp. 2851–2863, 2014.

[26] A. Vahidi, A. Stefanopoulou, and H. Peng, “Recursive least squares with

forgetting for online estimation of vehicle mass and road grade: theory and experiments," *Veh. Syst. Dyn.*, vol. 43, no. 1, pp. 31–55, 2005.

[27] V. Winstead and I. V. Kolmanovsky, "Estimation of road grade and vehicle mass via model predictive control," *Proc. 2005 IEEE Conf. Control Appl. 2005. CCA 2005.*, pp. 1588–1593, 2005.

[28] E. Raffone, "Road slope and vehicle mass estimation for light commercial vehicle using linear Kalman filter and RLS with forgetting factor integrated approach," *16th Int. Conf. Inf. Fusion*, pp. 1167–1172, 2013.

[29] N. Kidambi, R. L. Harne, Y. Fujii, G. M. Pietron, and K. W. Wang, "Methods in Vehicle Mass and Road Grade Estimation," *SAE Int. J. Passeng. Cars - Mech. Syst.*, vol. 7, no. 3, 2014.

[30] M. T. Breen, "System and Method for Determining Relative Vehicle Mass," United States Patent, 1996.

[31] H. Rieker, "Device for Determining the Mass of a Motor Vehicle,", United States Patent, 1990.

[32] H. H. Korst, R. A. White, and L. D. Metz, "Road Evaluation of the Aerodynamic Characteristics of Heavy Trucks," *SAE Int.*, no. 724, 2007.

[33] R. B. Carlson, J. Diez, and J. Gibbs, "The Measured Impact of Vehicle Mass on Road Load Forces and Energy Consumption for a BEV, HEV, and ICE Vehicle," *SAE Pap. No.*, vol. 2013-01–14, pp. 105–114, 2013.

[34] W. Mayer and J. Wiedemann, "Road Load Determination Based on Driving-Torque-Measurement," *SAE Int.*, 2014.

[35] R. Andersson, “Online Estimation of Rolling Resistance and Air Drag for Heavy Duty Vehicles,” KTH Industrial Engineering and Management, 2012.

[36] J. N. Barkenbus, “Eco-driving: An overlooked climate change initiative,” *Energy Policy*, vol. 38, no. 2, pp. 762–769, 2010.

[37] T. Wada, K. Yoshimura, S. I. Doi, H. Youhata, and K. Tomiyama, “Proposal of an eco-driving assist system adaptive to driver’s skill,” *IEEE Conf. Intell. Transp. Syst. Proceedings, ITSC*, no. 1, pp. 1880–1885, 2011.

[38] C. Vagg, C. J. Brace, D. Hari, S. Akehurst, J. Poxon, and L. Ash, “Development and field trial of a driver assistance system to encourage eco-driving in light commercial vehicle fleets,” *IEEE Trans. Intell. Transp. Syst.*, vol. 14, no. 2, pp. 796–805, 2013.

[39] K. Kondo and H. Goka, “Adaptive shift scheduling strategy introducing neural network in automatic transmission,” *JSAE*, vol. 16, pp. 411–414, 1995.

[40] C. Lin, H. Peng, and J. W. Grizzle, “A Stochastic Control Strategy for Hybrid Electric Vehicles,” *Am. Control Conf. 2004. Proc. 2004*, vol. 5, pp. 4710–4715 vol.5, 2004.

[41] R. Wang and S. M. Lukic, “Review of driving conditions prediction and driving style recognition based control algorithms for hybrid electric vehicles,” *2011 IEEE Veh. Power Propuls. Conf. VPPC 2011*, 2011.

[42] H. Yu, F. Tseng, and R. McGee, “Driving pattern identification for EV range estimation,” *2012 IEEE Int. Electr. Veh. Conf. IEVC 2012*, 2012.

[43] M. a S. Kamal, M. Mukai, J. Murata, and T. Kawabe, “On board eco-driving

system for varying road-traffic environments using model predictive control," *Proc. IEEE Int. Conf. Control Appl.*, pp. 1636–1641, 2010.

[44] F. Mensing, R. Trigui, and E. Bideaux, "Vehicle trajectory optimization for application in ECO-driving," *2011 IEEE Veh. Power Propuls. Conf. VPPC 2011*, 2011.

[45] C. Zhang and A. Vahidi, "Predictive Cruise Control with Probabilistic Constraints for Eco Driving," in *Proceedings of the ASME 2011 Dynamic Systems and Control Conference*, 2011, pp. 1–6.

[46] M. a Samad Kamal *et al.*, "Smart Driving of a Vehicle Using Model Predictive Control for Improving Traffic Flow," *Intell. Transp. Syst. IEEE Trans.*, vol. 15, no. 2, pp. 878–888, 2014.

[47] M. A. S. Kamal, M. Mukai, J. Murata, and T. Kawabe, "Ecological Vehicle Control on Roads With Up-Down Slopes," vol. 12, no. 3, pp. 783–794, 2011.

[48] M. Kerper, C. Wewetzer, H. Trompeter, W. Kiess, and M. Mauve, "Driving More Efficiently - The Use of Inter-Vehicle Communication to Predict a Future Velocity Profile," pp. 0–4, 2011.

[49] Wei-Yao Chou, Yi-Chun Lin, Yu-Hui Lin, and Syuan-Yi Chen, "Intelligent eco-driving suggestion system based on vehicle loading model," *2012 12th Int. Conf. ITS Telecommun.*, pp. 558–562, 2012.

[50] D. Vangi and A. Virga, "Evaluation of energy-saving driving styles for bus drivers," *Proc. Inst. Mech. Eng. Part D J. Automob. Eng.*, vol. 217, no. 4, pp. 299–305, 2005.

[51] V. Manzoni, A. Corti, P. De Luca, and S. M. Savaresi, “Driving style estimation via inertial measurements,” *IEEE Conf. Intell. Transp. Syst. Proceedings, ITSC*, pp. 777–782, 2010.

[52] C. D’Agostino, A. Saidi, G. Scouarnec, and L. Chen, “Learning-based driving events classification,” *IEEE Conf. Intell. Transp. Syst. Proceedings, ITSC*, no. Itsc, pp. 1778–1783, 2013.

[53] Y. Zhang, W. C. Lin, and Y. K. S. Chin, “A pattern-recognition approach for driving skill characterization,” *IEEE Trans. Intell. Transp. Syst.*, vol. 11, no. 4, pp. 905–916, 2010.

[54] G. S. Aoude, V. R. Desaraju, L. H. Stephens, and J. P. How, “Behavior classification algorithms at intersections and validation using naturalistic data,” *IEEE Intell. Veh. Symp. Proc.*, no. Iv, pp. 601–606, 2011.

[55] N. Oliver and A. P. Pentland, “Graphical models for driver behavior recognition in a SmartCar,” *Proc. IEEE Intell. Veh. Symp. 2000 (Cat. No.00TH8511)*, no. Mi, pp. 7–12, 2000.

[56] N. Kuge, T. Yamamura, O. Shimoyama, and A. Liu, “A Driver Behavior Recognition Method Based on a Driver Model Framework,” *Structure*, vol. 109, no. Idm, pp. 469–476, 2000.

[57] A. Sathyanarayana, B. Pinar, and J. H. L. Hansen, “Driver behavior analysis and route recognition by Hidden Markov Models,” *2008 IEEE Int. Conf. Veh. Electron. Saf.*, no. OCTOBER, 2008.

[58] Z. Constantinescu, C. Marinoiu, and M. Vladoiu, “Driving style analysis using

data mining techniques," *Int. J. Comput. Commun. Control*, vol. 5, no. 5, pp. 654–663, 2010.

[59] G. Kedar-Dongarkar and M. Das, "Driver classification for optimization of energy usage in a vehicle," *Procedia Comput. Sci.*, vol. 8, pp. 388–393, 2012.

[60] A. Doshi and M. M. Trivedi, "Tactical driver behavior prediction and intent inference: A review," *IEEE Conf. Intell. Transp. Syst. Proceedings, ITSC*, pp. 1892–1897, 2011.

[61] B. Higgs, M. Abbas, and A. Medina, "Analysis of the Wiedemann Car Following Model over Different Speeds using Naturalistic Data," *3rd Int. Conf. …*, pp. 1–22, 2011.

[62] J. Engstrom and T. Victor, "Real-time recognition of large-scale driving patterns," *ITSC 2001. 2001 IEEE Intell. Transp. Syst. Proc. (Cat. No.01TH8585)*, pp. 1018–1023, 2001.

[63] J. Carmona, F. García, D. Martín, A. Escalera, and J. Armingol, "Data Fusion for Driver Behaviour Analysis," *Sensors*, vol. 15, no. 10, pp. 25968–25991, 2015.

[64] T. Lee and Z. Filipi, "Real-World Driving Pattern Recognition for Adaptive HEV Supervisory Control : Based on Representative Driving Cycles in Midwestern US," 2012.

[65] Y. L. Murphey, R. Milton, and L. Kiliaris, "Driver's style classification using jerk analysis," *2009 IEEE Work. Comput. Intell. Veh. Veh. Syst. CIVVS 2009 - Proc.*, pp. 23–28, 2009.

[66] E. Ericsson, "Independent driving pattern factors and their influence on fuel-use

and exhaust emission factors," *Transp. Res. Part D Transp. Environ.*, vol. 6, no. 5, pp. 325–345, 2001.

[67] Z. Liu, A. Ivanco, and Z. Filipi, "Quantification of Drive Cycle's Rapid Speed Fluctuations Using Fourier Analysis," *SAE Int. J. Altern. Powertrains*, vol. 4, no. 1, 2015.

[68] C. Miyajima *et al.*, "Driver modeling based on driving behavior and its evaluation in driver identification," *Proc. IEEE*, vol. 95, no. 2, pp. 427–437, 2007.

[69] E. Ericsson, "Variability in urban driving patterns," *Transp. Res. Part D Transp. Environ.*, vol. 5, no. 5, pp. 337–354, 2000.

[70] K. Hayashi, Y. Shimizu, Y. Dote, A. Takayama, and A. Hirako, "Neuro fuzzy transmission control for automobile with variable loads," *IEEE Trans. Control Syst. Technol.*, vol. 3, no. 1, pp. 49–52, 1995.

[71] S Sakaguchi, I. Sakai, and T. Haga., "Application of Fuzzy Logic to Shift Scheduling Method for Automatic Transmission," *Second IEEE Int. Conf.*, 1993.

[72] W. Jun, Q. Wang, P. Wang, and L. Li, "Adaptive Shift Control Strategy Based On Driving Style Recognition," *SAE Int.*, 2013.

[73] X. Yin and J. Tan, "Research on a Neural Network Model Based Automatic Shift Schedule with Dynamic 3-Parameters," *Engineering*, no. 724, 2005.

[74] S. Ha and H. Jeon, "Development of Intelligent Gear-Shifting Map Based on Radial Basis Function Neural Networks," vol. 13, no. 2, pp. 116–123, 2013.

[75] D. Kim, H. Peng, S. Bai, and J. M. Maguire, "Control of integrated powertrain with electronic throttle and automatic transmission," *IEEE Trans. Control Syst.*

Technol., vol. 15, no. 3, pp. 474–482, 2007.

[76] E. Hellström, J. Åslund Jan, and L. Nielsen, “Design of an efficient algorithm for fuel-optimal look-ahead control,” *Control Eng. Pract.*, vol. 18, no. 11, pp. 1318–1327, 2010.

[77] V. Ngo, T. Hofman, M. Steinbuch, and A. Serrarens, “Predictive gear shift control for a parallel Hybrid Electric Vehicle,” *2011 IEEE Veh. Power Propuls. Conf.*, pp. 1–6, 2011.

[78] V. D. Ngo, J. a. Colin Navarrete, T. Hofman, M. Steinbuch, and a. Serrarens, “Optimal gear shift strategies for fuel economy and driveability,” *Proc. Inst. Mech. Eng. Part D J. Automob. Eng.*, vol. 227, no. 10, pp. 1398–1413, 2013.

[79] Z. Yong and S. Jian, “Automatic Transmission Shift Point Control Under Different Driving Vehicle Mass,” *Sae Tech. Pap. Ser.*, vol. 2002, no. 2002-01–1258, 2002.

[80] D. Le Guen, T. Weck, A. Balihe, and B. Verbeke, “Definition of Gearshift Pattern: Innovative Optimization Procedures Using System Simulation,” *SAE Int. J. Fuels Lubr.*, vol. 4, no. 1, pp. 412–431, 2011.

[81] P. Liu, T. Zhang, and X. Zhao, “Vehicle Drivability Evaluation and Pedal-acceleration Response Analysis,” *Int. J. Adv. Inf. Sci. Serv. Sci.*, vol. 5, no. 10, pp. 506–513, 2013.

[82] R. E. Dorey and C. B. Holmes, “Vehicle Driveability - Its Characterisation and Measurement,” *SAE Tech. Pap.*, no. 1999-01–0949, 1999.

[83] R. E. Dorey and E. J. Martin, “Vehicle Driveability — The Development of an Objective Methodology,” *SAE Tech. Pap. 2000-01-1326*, no. 724, 2000.

[84] V. Wicke, C. J. Brace, M. Deacon, and N. D. Vaughan, “Preliminary Results from Driveability Investigations of Vehicles with Continuously Variable Transmissions,” vol. 5, pp. 9–14, 1999.

[85] X. Wei and G. Rizzoni, “Objective Metrics of Fuel Economy, Performance and Driveability – A Review,” *SAE Tech. Pap.*, vol. 2004, no. 2004-01–1338, 2004.

[86] L. Guzzella and A. Sciarretta, *Vehicle Propulsion Systems: Introduction to Modeling and Optimization*. Springer Science & Business Media, 2012.

[87] B. M. Redrouthu and S. Das, “Tyre modelling for rolling resistance,” Chalmers University of Technology, 2014.

[88] W. Navidi, *Statistics for Engineers and Scientists*, 4 edition. McGraw-Hill Education, 2014.

[89] K. J. Astrom and D. B. Wittenmark, *Adaptive Control*, Second Edi. Prentice Hall, 1994.

[90] M. R. Stepper, “J1939 High Speed Serial Communications , The Next Generation Network for Heavy Duty Vehicles,” *SAE Int.*, 1993.

[91] G. J. Thompson, N. N. Clark, M. Gautam, D. K. Carder, and D. W. Lyons, “Inference of Torque and Power from Heavy-Duty Diesel Engines for On-Road Emissions Monitoring,” *Communication*, no. 724, 2002.

[92] National Research Council, *Tires And Passenger Vehicle Fuel Economy*. 2006.

[93] I. Hucho, *Aerodynamics of Road Vehicles*, vol. 25, no. 1. 1993.

[94] SAE, *Road Load Measurement Using Onboard Anemometry and Coastdown Techniques*. 2014, p. 2263.

[95] M. a. S. Kamal, M. Mukai, J. Murata, and T. Kawabe, “Ecological driver assistance system using model-based anticipation of vehicle–road–traffic information,” *IET Intell. Transp. Syst.*, vol. 4, no. 4, p. 244, 2010.

[96] R. Wang and S. M. Lukic, “Review of driving conditions prediction and driving style recognition based control algorithms for hybrid electric vehicles,” *Veh. Power Propuls. Conf. (VPPC), 2011 IEEE*, pp. 1–7, 2011.

[97] A. Duran and K. Walkowicz, “A Statistical Characterization of School Bus Drive Cycles Collected via Onboard Logging Systems,” *SAE Int. 2013-01-2400*, pp. 400–406, 2013.

[98] J. Lin, E. Keogh, S. Lonardi, and B. Chiu, “A Symbolic Representation of Time Series, with Implications for Streaming Algorithms,” *Proc. 8th ACM SIGMOD Work. Res. Issues Data Min. Knowl. Discov.*, pp. 2–11, 2003.

[99] K. S. Fu, *Syntactic Pattern Recognition, Applications*. 1981.

[100] S. Verwer, M. De Weerdt, and C. Witteveen, “Learning driving behavior by timed syntactic pattern recognition,” *IJCAI Int. Jt. Conf. Artif. Intell.*, pp. 1529–1534, 2011.

[101] J. Lin and D. a. Niemeier, “An exploratory analysis comparing a stochastic driving cycle to California’s regulatory cycle,” *Atmos. Environ.*, vol. 36, no. 38, pp. 5759–5770, 2002.

[102] “The golden rules of ecodriving.” [Online]. Available: http://www.ecodrive.org/en/what_is_ecodriving-/the_golden_rules_of_ecodriving/.

[103] C. Bishop and N. Nasrabadi, *Pattern recognition and machine learning*. Springer, 2007.

[104] R. Nasdal and M. Link, “GALOP - IAV ’ s Universal Speed Ratio Selection Strategy for ATs , CVTs and Hybrid Drivetrains,” vol. 2002, no. 724, 2002.

[105] A. Ivanco and Z. Filipi, “Vehicle Modeling and Evaluation of the Engine Options in Conventional and Mild-Hybrid Powertrain,” 2013.

[106] A. Hoekstra, D. Filev, S. Szwabowski, K. McDonough, and I. Kolmanovsky, “Evolving Markov chain models of driving conditions using onboard learning,” *2013 IEEE Int. Conf. Cybern. CYBCONF 2013*, pp. 1–6, 2013.

[107] J. Shlens, “A tutorial on principal component analysis,” *Internet Artic.*, pp. 1–13, 2005.

[108] F. Assadian, G. Mohan, and S. Longo, “Comparative analysis of forward-facing models vs backward-facing models in powertrain component sizing,” *Hybrid Electr. Veh. Conf. 2013 (HEVC 2013)*, vol. 2013, no. 621 CP, p. 10.7-10.7, 2013.

[109] I. I. Delice and S. Ertugrul, “Intelligent Modeling of Human Driver: A Survey,” *2007 IEEE Intell. Veh. Symp.*, pp. 648–651, 2007.

[110] J. J. Moskwa and J. K. Hedrick, “Automotive Engine Modeling for Real Time Control Application,” *Am. Control Conf. 1987*, pp. 341–346, 1987.

[111] V. Larsson *et al.*, “Commuter Route Optimized Energy Management of Hybrid Electric Vehicles,” *Intell. Transp. Syst. IEEE Trans.*, vol. 15, no. 3, pp. 1145–1154, 2014.

[112] Z. Chen, A Vahidi, P. Pisu, L. Xiaopeng, and K. Tennant, “Role of Terrain

Preview in Energy Management of Hybrid Electric Vehicles," *Veh. Technol. IEEE Trans.*, vol. 59, no. 3, pp. 1139–1147, 2010.

[113] C. Zhang and A. Vahidi, "Real-time optimal control of plug-in hybrid vehicles with trip preview," *2010 Am. Control Conf.*, pp. 6917–6922, 2010.

[114] C. Zhang and A. Vahidi, "Route preview in energy management of plug-in hybrid vehicles," *IEEE Trans. Control Syst. Technol.*, vol. 20, no. 2, pp. 546–553, 2012.

[115] A. Rezaei and J. B. Burl, "Prediction of Vehicle Velocity for Model Predictive Control," *IFAC-PapersOnLine*, vol. 48, no. 15, pp. 257–262, 2015.

[116] T. Cummings, T. H. Bradley, and Z. D. Asher, "The effect of trip preview prediction signal quality on hybrid vehicle fuel economy," *IFAC Proc. Vol.*, vol. 48, no. 15, pp. 271–276, 2015.

[117] I. V. Kolmanovsky and D. P. Filev, "Terrain and traffic optimized vehicle speed control," *IFAC Proc. Vol.*, pp. 378–383, 2010.

[118] K. McDonough *et al.*, "Modeling of vehicle driving conditions using transition probability models," *Proc. IEEE Int. Conf. Control Appl.*, vol. 1, no. 4, pp. 544–549, 2011.

[119] K. McDonough, I. Kolmanovsky, D. Filev, D. Yanakiev, S. Szwabowski, and J. Michelini, "Stochastic dynamic programming control policies for fuel efficient in-traffic driving," *Am. Control Conf. (ACC), 2012*, no. 734, pp. 3986–3991, 2012.

[120] M. S. Kamal, M. Mukai, J. Murata, and T. Kawabe, "Development of Ecological Driving System Using Model Predictive Control," *Sci. Technol.*, pp. 3549–3554, 2009.

[121] Y. Chen, D. Zhang, and K. Li, “Enhanced eco-driving system based on V2X communication,” *IEEE Conf. Intell. Transp. Syst. Proceedings, ITSC*, pp. 200–205, 2012.

[122] K. Mcdonough, I. Kolmanovsky, D. Filev, D. Yanakiev, and S. Szwabowski, “Stochastic Dynamic Programming Control Policies for Fuel Efficient Vehicle Following,” *Am. Control Conf.*, pp. 1350–1355, 2013.